Maximum elastic deformations of relativistic stars

Nathan K. Johnson-McDaniel and Benjamin J. Owen

Maximum elastic deformations of relativistic stars

Nathan K. Johnson-McDaniel[1,2] and Benjamin J. Owen[1]

[1]*Institute for Gravitation and the Cosmos, Center for Particle and Gravitational Astrophysics,*
Department of Physics, The Pennsylvania State University, University Park, PA 16802, USA
[2]*Theoretisch-Physikalisches Institut, Friedrich-Schiller-Universität, Max-Wien-Platz 1, 07743 Jena, Germany*

We present a method for calculating the maximum elastic quadrupolar deformations of relativistic stars, generalizing the previous Newtonian, Cowling approximation integral given by [G. Ushomirsky *et al.*, Mon. Not. R. Astron. Soc. **319**, 902 (2000)]. (We also present a method for Newtonian gravity with no Cowling approximation.) We apply these methods to the $m = 2$ quadrupoles most relevant for gravitational radiation in three cases: crustal deformations, deformations of crystalline cores of hadron–quark hybrid stars, and deformations of entirely crystalline color superconducting quark stars. In all cases, we find suppressions of the quadrupole due to relativity compared to the Newtonian Cowling approximation, particularly for compact stars. For the crust these suppressions are up to a factor of ~ 6, for hybrid stars they are up to ~ 4, and for solid quark stars they are at most ~ 2, with slight enhancements instead for low mass stars. We also explore ranges of masses and equations of state more than in previous work, and find that for some parameters the maximum quadrupoles can still be very large. Even with the relativistic suppressions, we find that $1.4\,M_\odot$ stars can sustain crustal quadrupoles of a few $\times\, 10^{39}$ g cm^2 for the SLy equation of state, or close to 10^{40} g cm^2 for equations of state that produce less compact stars. Solid quark stars of $1.4\,M_\odot$ can sustain quadrupoles of around 10^{44} g cm^2. Hybrid stars typically do not have solid cores at $1.4\,M_\odot$, but the most massive ones ($\sim 2\,M_\odot$) can sustain quadrupoles of a few $\times\, 10^{41}$ g cm^2 for typical microphysical parameters and a few $\times\, 10^{42}$ g cm^2 for extreme ones. All of these quadrupoles assume a breaking strain of 10^{-1} and can be divided by 10^{45} g cm^2 to yield the fiducial "ellipticities" quoted elsewhere.

I. INTRODUCTION

Shortly after the discovery of pulsars and the realization that they are rotating neutron stars, deformations of rotating neutron stars were proposed as sources of continuous gravitational radiation [1–4]; see [5] for an early review. Searches for such radiation are an ongoing concern of the LIGO and Virgo gravitational wave detectors [6–8]; see [9–11] for recent reviews. It is thus of great interest to know the maximum quadrupolar deformation that a neutron star could sustain, in order to motivate further searches and help interpret upper limits or detections. In the case of elastic (as opposed to magnetic) deformations, the main factor influencing the answer is whether the neutron star contains particles more exotic than neutrons [9, 12]. However, the structure of the star also plays an important role.

While there are relativistic calculations of the quadrupole deformations due to magnetic fields (e.g., [13–17]), all the computations involving elastic deformations have used Newtonian gravity. Moreover, all but two of these computations have used the integral expression obtained in the Cowling approximation (i.e., neglecting the self-gravity of the perturbation) by Ushomirsky, Cutler, and Bildsten (UCB) [18]; see [12, 19–21]. Haskell, Jones, and Andersson (HJA) [22] dropped the Cowling approximation using a somewhat different formalism than UCB's; there is a further application of their results in [23].

We improve these treatments by generalizing the UCB integral to relativistic gravity with no Cowling approximation. We also provide a similar generalization for the Newtonian no-Cowling case, as a warm-up. In addition to providing a simpler formalism for performing computations than the more general Newtonian gravity treatment in HJA, the integrals we obtain allow us to verify that a maximal uniform strain continues to yield the maximum quadrupole deformation in the Newtonian and relativistic no-Cowling cases. (UCB showed this to be true for an arbitrary equation of state in the Newtonian Cowling approximation case; we are able to verify that it is true in the more general cases for each background stellar model we consider.)

We then apply our calculation to the standard case of quadrupoles supported by shearing the lattice of nuclei in the crust, as well as the cases where the quadrupole is supported by the hadron–quark mixed phase lattice in the core, or a crystalline color superconducting phase throughout a solid strange quark star. For the crustal quadrupoles, we calculate the shear modulus following HJA, using the equation of state (EOS) and composition results of Douchin and Haensel [24] and the effective shear modulus calculated by Ogata and Ichimaru [25]. (There are recent improvements to the Ogata and Ichimaru result [26–28], but these only reduce their shear modulus by $< 10\%$.) For the hadron–quark mixed phase, we use our recent calculations of the EOS and shear modulus [29] for a variety of parameters. (We also consider the range of surface tensions for which the mixed phase is favored.) For crystalline quark matter, we use the shear modulus calculated by Mannarelli, Rajagopal,

and Sharma [30], and the EOS given by Kurkela, Romatschke, and Vuorinen [31].

In all cases, we use a breaking strain of 0.1, comparable to that calculated by Horowitz and Kadau [32] using molecular dynamics simulations. (Hoffman and Heyl [33] have recently obtained very similar values over more of parameter space.) This result is directly applicable to the crustal lattice, at least for the outer crust, above neutron drip (though see Chugunov and Horowitz [34] for caveats). We also feel justified in applying it to the inner crust, as well as to the mixed phase and crystalline quark matter, since the primary source of the high breaking strain appears to be the system's large pressure. But one can apply our results to any breaking strain using the linear scaling of the maximum quadrupole with breaking strain.

In our general relativistic calculation, we use the relativistic theory of elasticity given by Carter and Quintana [35] and placed in a more modern guise by Karlovini and Samuelsson [36]. However, all we need from it is the relativistic form of the elastic stress-energy tensor, which can be obtained by simple covariance arguments, as noted by Schumaker and Thorne [37]. We also use the standard Thorne and Campolattaro [38] Regge-Wheeler gauge [39] formalism for perturbations of static relativistic stars, following Hinderer's recent calculation [40] of the quadrupole moment of a tidally deformed relativistic star (first discussed in Flanagan and Hinderer [41]), and the classic calculation by Ipser [42].

Even though we are interested in the gravitational radiation emitted by rotating stars, it is sufficient for us to calculate the static quadrupole deformation. As discussed by Ipser [42], and then proved for more general situations by Thorne [43], this static quadrupole (obtained from the asymptotic form of the metric) can be inserted into the quadrupole formula to obtain the emitted gravitational radiation in the fully relativistic, slow-motion limit. [This approximation has uncontrolled remainders of order $(\omega/\omega_K)^2$, where ω and ω_K are the star's angular velocity and its maximum—i.e., Kepler—angular velocity, respectively. This ratio is $\lesssim 10^{-2}$ for the pulsars for which LIGO has been able to beat the spin-down limit [6].]

We shall generally show the gravitational constant G and speed of light c explicitly, though we shall take $G = c = 1$ in most of Sec. III, only restoring them in our final expressions. The relativistic calculation was aided by use of the computer algebra system MAPLE and the associated tensor manipulation package GRTENSORII [44]. We used MATHEMATICA 7 to perform numerical computations.

The paper is structured as follows: In Sec. II, we review UCB's formalism and extend it by introducing a Green function to compute the maximum Newtonian quadrupole deformation without making the Cowling approximation. In Sec. III, we further generalize to the fully relativistic case, and compare the various approximations for the maximum quadrupole. In Sec. IV,

we show the maximum quadrupoles for three different cases: first crustal quadrupoles, then hadron–quark hybrid quadrupoles, and finally solid strange quark star quadrupoles. We also describe the modifications to our formalism needed to treat solid strange quark stars. We discuss all these results in Sec. V, and summarize and conclude in Sec. VI. In the Appendix, we show that the mixed phase is favored by global energy arguments even for surface tensions large enough that it is disfavored by local energy arguments.

II. NEWTONIAN CALCULATION OF THE MAXIMUM QUADRUPOLE

We first demonstrate how to compute the maximum Newtonian quadrupole without making the Cowling approximation. This provides a warm-up before we tackle the full relativistic case, and also allows us to verify some of the statements made by UCB and HJA. We use the basic formalism of UCB, modeling the star as nonrotating, with the stress-energy tensor of a perfect fluid plus shear terms, and treating the shear contributions as a first-order perturbation of hydrostatic equilibrium. This perturbative treatment should be quite a good approximation: The maximum shear stress to energy density ratio we consider in the crustal and hybrid star cases is $\lesssim 0.05\%$ (and the maximum shear stress to pressure ratio is $\lesssim 0.3\%$). (Here we have taken the shear stress to be $\mu\bar{\sigma}_{\max}$, which is good up to factors of order unity.) And even in the case of solid strange quark stars, the maximum shear stress to energy density ratio is still only at most $\sim 0.2\%$. [We have already discussed the effects of rotation in the relativistic case, above; UCB note at the beginning of their Sec. 4 that rotation also only modifies the perturbative Newtonian results for the static deformations we and they consider at the $O([\omega/\omega_K]^2)$ level.]

It is convenient to start by writing the quadrupole moment in terms of the surface value of the perturbation to the star's Newtonian potential. We start from UCB's definition of

$$Q_{22} := \int_0^\infty \delta\rho(r) r^4 dr \qquad (1)$$

[where the (Eulerian) density perturbation $\delta\rho$ and all similar perturbed quantities have only an $l = m = 2$ spherical harmonic component]. [Note that this quadrupole moment differs by an overall constant from the one defined by Thorne [43]—e.g., his Eq. (5.27a).] We then recall that the perturbed Poisson equation for the $l = 2$ part of the perturbed gravitational potential is

$$(\triangle_2 \delta\Phi)(r) := \frac{1}{r^2}[r^2 \delta\Phi'(r)]' - \frac{6}{r^2}\delta\Phi(r) = 4\pi G\delta\rho \qquad (2)$$

($\triangle_2$ is the $l = 2$ radial part of the Laplacian), with boundary conditions of

$$\delta\Phi(0) = 0, \qquad R\delta\Phi'(R) = -3\delta\Phi(R), \qquad (3)$$

where R is the radial coordinate of the star's surface. [See, e.g., Eqs. (2.15) and (2.16) in [45]—their Φ_{22} is our $\delta\Phi$. Note also that the primes denote derivatives with respect to r. Additionally, we shall continue to be inconsistent with our inclusion of the functional dependence of quantities—e.g., $\delta\rho$ depends upon r, even though we do not always indicate this explicitly. We will eventually stop displaying $\delta\Phi$'s explicit functional dependence on r, for instance.] If we now substitute Eq. (2) into Eq. (1) and integrate by parts using the boundary conditions (3), we obtain

$$Q_{22} = -\frac{5R^3}{4\pi G}\delta\Phi(R). \quad (4)$$

This sort of expression is more commonly seen in the relativistic case, where it is necessary to obtain the quadrupole in this manner by looking at the perturbation's asymptotic behavior—see the discussion in Sec. III.

We now wish to obtain an equation for $\delta\Phi$ in terms of the shear stresses. We follow UCB in decomposing the perturbed stress tensor as [see their Eqs. (59) and (61)]

$$\delta\tau_{ab} = -\delta p Y_{lm} g_{ab} + t_{rr} Y_{lm}(\hat{r}_a\hat{r}_b - e_{ab}/2) + t_{r\perp}f_{ab} \\ + t_\Lambda(\Lambda_{ab} + Y_{lm}e_{ab}/2). \quad (5)$$

Here δp is the (Eulerian) pressure perturbation; Y_{lm} is a spherical harmonic; $\hat{r}_a$ is the radial unit vector; t_{rr}, $t_{r\perp}$, and t_Λ are the components of the shear stresses; and g_{ab} denotes the metric of flat, 3-dimensional Euclidean space. (Following UCB, we will generally write out l and m explicitly, even though we only consider $l = m = 2$ here.) Also [Eqs. (40) in UCB],

$$e_{ab} := g_{ab} - \hat{r}_a\hat{r}_b, \quad (6a)$$
$$f_{ab} := 2r\hat{r}_{(a}\nabla_{b)}Y_{lm}/\beta, \quad (6b)$$
$$\beta := \sqrt{l(l+1)} = \sqrt{6}, \quad (6c)$$
$$\Lambda_{ab} := r^2\nabla_a\nabla_b Y_{lm}/\beta^2 + f_{ab}/\beta. \quad (6d)$$

(We have corrected the dropped factor of β^{-1} multiplying f_{ab} in UCB's definition of Λ_{ab}—this was also noticed by HJA.) We also have

$$t_{ab} = 2\mu\sigma_{ab}, \quad (7)$$

where μ is the shear modulus and σ_{ab} is the strain tensor. (This is a factor-of-2 correction to the expression in UCB, as noted in [12].) Now, a convenient expression can be obtained from the perturbed equation of hydrostatic equilibrium

$$\nabla^a\delta\tau_{ab} = \delta\rho g(r)\hat{r}_b + \rho\nabla_b\delta\Phi \quad (8)$$

(∇_a denotes the flat-space covariant derivative), by substituting for $\delta\rho$ using the Poisson equation (2) and projecting along $\hat{r}^b$, yielding

$$\frac{\triangle_2\delta\Phi}{4\pi G} + \frac{\rho}{g(r)}\delta\Phi' = \frac{\hat{r}^b\nabla^a\delta\tau_{ab}}{g(r)} \\ = \frac{1}{g(r)}\left[-\delta p' + t'_{rr} + \frac{3}{r}t_{rr} - \frac{\beta}{r}t_{r\perp}\right]. \quad (9)$$

We then project Eq. (8) along $\nabla^b Y_{lm}$ to express δp in terms of the shear stresses t_{rr}, $t_{r\perp}$, and t_Λ, along with ρ and $\delta\Phi$, giving

$$\delta p = -\rho\delta\Phi - \frac{t_{rr}}{2} + \frac{r}{\beta}t'_{r\perp} + \frac{3}{\beta}t_{r\perp} + \left(\frac{1}{\beta^2} - \frac{1}{2}\right)t_\Lambda. \quad (10)$$

Substituting this into Eq. (9), we thus obtain

$$\triangle_2\delta\Phi - \frac{4\pi G}{g(r)}\rho'\delta\Phi = \frac{4\pi G}{g(r)}\left[\frac{3}{2}t'_{rr} - \frac{4}{\beta}t'_{r\perp} - \frac{r}{\beta}t''_{r\perp} \\ - \left(\frac{1}{\beta^2} - \frac{1}{2}\right)t'_\Lambda + \frac{3}{r}t_{rr} - \frac{\beta}{r}t_{r\perp}\right]. \quad (11)$$

We now wish to obtain an integral expression for Q_{22} that generalizes UCB's Eq. (64) to the case where we do not make the Cowling approximation. We shall do this by obtaining the Green function for the left-hand side of Eq. (11) and then integrating by parts. We will be able to discard all of the boundary terms, since the stresses vanish at the star's surface (we assume that the shear modulus vanishes there) and the integrand vanishes at the star's center. We can obtain the Green function using the standard Sturm-Liouville expression in terms of the solutions of the homogeneous equation [e.g., Eq. (10.103) in Arfken and Weber [46]]. We obtain the appropriate solution to the homogeneous equation numerically for a given background stellar model (EOS and mass). The equation for the Green function is [multiplying the left-hand side of Eq. (11) by r^2 to improve its regularity]

$$(\mathcal{L}_N\mathcal{G})(r,\bar{r}) := \frac{\partial}{\partial r}\left[r^2\frac{\partial}{\partial r}\mathcal{G}(r,\bar{r})\right] - \left[6 + \frac{4\pi Gr^2}{g(r)}\rho'\right]\mathcal{G}(r,\bar{r}) \\ = \delta(r - \bar{r}) \quad (12)$$

[$\delta(r - \bar{r})$ is the Dirac delta function], with boundary conditions (at the star's center and surface) of

$$\mathcal{G}(0,\bar{r}) = 0, \qquad R\partial_1\mathcal{G}(R,\bar{r}) = -3\mathcal{G}(R,\bar{r}), \quad (13)$$

where ∂_1 denotes a partial derivative taken with respect to the first "slot" of the function.

If we then write [using Eq. (4), the factor of r^2 from the Green function equation (12), and the prefactor on the right-hand side of Eq. (11)]

$$G_N(r) := -5R^3 r^2\mathcal{G}(R,r)/g(r), \quad (14)$$

we have

$$Q_{22}^N = \int_0^R G_N(r) \left[\frac{3}{2}t'_{rr} - \frac{4}{\beta}t'_{r\perp} - \frac{r}{\beta}t''_{r\perp} - \left(\frac{1}{\beta^2} - \frac{1}{2} \right) t'_\Lambda + \frac{3}{r}t_{rr} - \frac{\beta}{r}t_{r\perp} \right] dr$$

$$= -\int_0^R \left\{ \left[\frac{3}{2}G'_N(r) - \frac{3}{r}G_N(r) \right] t_{rr} + \left[\frac{r}{\beta}G''_N(r) - \frac{2}{\beta}G'_N(r) + \frac{\beta}{r}G_N(r) \right] t_{r\perp} + \left(\frac{1}{2} - \frac{1}{\beta^2} \right) G'_N(r) t_\Lambda \right\} dr. \tag{15}$$

We have freely integrated by parts in obtaining the second expression, noting that the boundary terms are zero since $G_N(r)$ vanishes sufficiently rapidly as $r \to 0$ and the stresses are zero at the surface of the star (since we assume that the shear modulus vanishes at the star's surface).[1] This reduces to UCB's Eq. (64) if we take the Cowling approximation

$$G_N(r) \to r^4/g(r), \tag{16}$$

corresponding to dropping the second term on the left-hand side of Eq. (11).

To obtain an analogue of the expression for the maximum quadrupole given in Eq. (5) of Owen [12], we note that UCB's argument about maximum uniform strain leading to the maximum quadrupole still holds here for the stars we consider, since the coefficients of the stress components in the integrand are all uniformly positive. (We have checked this numerically for each background stellar model we consider.) The strain tensor components are

$$\sigma_{rr} = (32\pi/15)^{1/2}\bar{\sigma}_{\max}, \tag{17a}$$

$$\sigma_{r\perp} = (3/2)^{1/2}\sigma_{rr}, \tag{17b}$$

$$\sigma_\Lambda = 3\sigma_{rr} \tag{17c}$$

in the case where the star is maximally (and uniformly) strained—see Eqs. (67) in UCB. The breaking strain $\bar{\sigma}_{\max}$ is given by the von Mises expression,

$$\sigma_{ab}\sigma^{ab} = 2\bar{\sigma}_{\max}^2. \tag{18}$$

It thus corresponds to assuming that the lattice yields when it has stored a certain maximum energy density. We then have

$$\frac{|Q_{22}^{\max,N}|}{\bar{\sigma}_{\max}} = \sqrt{\frac{32\pi}{15}} \int_0^R \mu(r) \left[rG''_N(r) + 3G'_N(r) \right] dr. \tag{19}$$

---

[1] We shall treat the case where the stresses do *not* vanish at the surface of the star when we consider solid strange quark stars in Sec. IV C. Also, note that HJA claim that UCB's expression does not include distributional contributions due to sudden changes in the shear modulus. This is not the case—these are included due to UCB's integration by parts (cf. the definition of the distributional derivative). All that the UCB derivation requires is, e.g., that the shear modulus vanish outside of the crust, not that it do so continuously.

This reduces to Eq. (5) in Owen [12] if we use the Cowling approximation (16).

Note that there is no direct contribution from ρ' to G''_N in the no-Cowling case, despite what one might expect from Eq. (12): Writing $\bar{\mathcal{G}}(r) := \mathcal{G}(R,r)$ for notational simplicity, the ρ' contribution from

$$\bar{\mathcal{G}}''(r) = (2/r)\bar{\mathcal{G}}'(r) + [6/r^2 + 4\pi G\rho'(r)/g(r)]\bar{\mathcal{G}}(r) \tag{20}$$

is exactly canceled by one from

$$g''(r) = 6Gm(r)/r^4 - 8\pi G\rho(r)/r + 4\pi G\rho'(r) \tag{21}$$

in

$$G''_N(r) = -5R^3r^2[\bar{\mathcal{G}}''(r)/g(r) - \bar{\mathcal{G}}(r)g''(r)/\{g(r)\}^2] + \{\text{terms with no } \rho'\}. \tag{22}$$

However, there is a direct contribution from ρ' to G''_N (via g'') if we make the Cowling approximation [Eq. (16)]. We shall see that this leads to a significant difference in the resulting contributions to the quadrupole moment from regions of the star surrounding a sudden change in density (e.g., near the crust-core interface, which will be relevant for the quadrupoles supported by crustal elasticity considered by UCB and others).

Numerically, we compute G_N using the standard expression for the Green function in terms of the two independent solutions to the homogeneous equation [see, e.g., Eq. (10.103) in Arfken and Weber [46]]. Since we are solely interested in the Green function evaluated at the star's surface, we can eliminate one of the homogeneous solutions using the boundary conditions there, and only consider the homogeneous solution that is regular at the origin, which we call F. In terms of F, the Green function is given by

$$\mathcal{G}(R,r) = -\frac{F(r)}{3RF(R) + R^2F'(R)}. \tag{23}$$

We thus solve $\mathcal{L}_N F = 0$ [with the operator $\mathcal{L}_N$ given by Eq. (12)] with the boundary conditions $F(r_0) = 1$ and $F'(r_0) = 2/r_0$, where r_0 is the small inner radius used in the solution of the OV equations, as discussed at the end of Sec. III. [These boundary conditions come from regularity at the origin, which implies that $F(r) = O(r^2)$ there.]

Our Green function method for obtaining the maximum quadrupole numerically may seem more complicated than existing methods because it introduces extra

steps. However this method is ideal for showing that maximum stress gives the maximum quadrupole and for seeing how much stresses at different radii contribute to the total quadrupole. It also appears to be the simplest way of dealing with any potential distributional contributions from the derivatives of the shear modulus, since they are automatically taken care of by the integration by parts.

III. GENERAL RELATIVISTIC CALCULATION OF THE MAXIMUM QUADRUPOLE

Here we compute the maximum quadrupole moment in general relativity, using the Regge-Wheeler gauge [39] relativistic stellar perturbation theory developed by Thorne and Campolattaro [38], as in the similar calculation of the tidal Love number of a relativistic star by Hinderer [40]. We start by writing down the line element corresponding to a static, even-parity, $l = 2$ first-order perturbation of a static, spherical, relativistic star in the Regge-Wheeler gauge [cf. Eq. (14) in Hinderer [40]]:

$$ds^2 = -[1 + H_0(r)Y_{lm}]f(r)dt^2 + [1 + H_2(r)Y_{lm}]h(r)dr^2$$
$$+ [1 + K(r)Y_{lm}]r^2(d\theta^2 + \sin^2\theta d\phi^2). \tag{24}$$

Here we have used the notation of Wald [47] for the background, so that f and h are the standard Schwarzschild functions for the unperturbed star, with $f = e^{2\phi}$, where

$$\phi'(r) = \frac{m(r) + 4\pi r^3 p}{r[r - 2m(r)]}, \tag{25}$$

with $\phi(R) = \log(1 - 2M/R)/2$, and

$$h(r) = \left[1 - \frac{2m(r)}{r}\right]^{-1}. \tag{26}$$

In these expressions,

$$m(r) := 4\pi \int_0^r \rho(\bar{r})\bar{r}^2 d\bar{r}. \tag{27}$$

Also, recall that we write our spherical harmonics in terms of l and m, following UCB, even though we specialized to $l = m = 2$, and that we are now taking $G = c = 1$.

The metric perturbation is determined by H_0, H_2, and K, which here are sourced by the perturbation to the star's stress-energy tensor. The appropriate stress-energy tensor can be obtained directly from the standard Newtonian expression (5) by simple covariance arguments, as in Schumaker and Thorne [37], or from the detailed relativistic elasticity theory of Carter and Quintana [35] [see their Eq. (6.19); this is also given in Eq. (128) of Karlovini and Samuelsson [36]]. All we really need for our purposes is to note that the shear contribution is tracefree with respect to the background metric, so that

we can use the obvious covariant generalization of the decomposition given by UCB,[2] yielding

$$\delta T_{ab} = [\delta\rho\hat{t}_a\hat{t}_b + \delta p(g_{ab} + \hat{t}_a\hat{t}_b) - t_{rr}(\hat{r}_a\hat{r}_b - q_{ab}/2)]Y_{lm}$$
$$- t_{r\perp}f_{ab} - t_\Lambda(\tilde{\Lambda}_{ab} + h^{1/2}Y_{lm}q_{ab}/2), \tag{28}$$

with the full stress-energy tensor given by

$$T_a{}^b = \rho\hat{t}_a\hat{t}^b + p(\delta_a{}^b + \hat{t}_a\hat{t}^b) + \delta T_a{}^b. \tag{29}$$

Here, indices now run over all four spacetime dimensions and g_{ab} denotes the background (spacetime) metric (which we use to raise and lower indices). Additionally, we have introduced the background temporal and radial unit vectors $\hat{t}_a$ and $\hat{r}_a$; q_{ab} is the induced metric on the unit 2-sphere; $f_{ab} := 2r\hat{r}_{(a}\nabla_{b)}Y_{lm}/\beta$; and $\tilde{\Lambda}_{ab} := r^2h^{1/2}\nabla_a\nabla_bY_{lm}/\beta^2 + f_{ab}/\beta$. Here $\hat{r}_a$ and ∇_a now have their curved-space meanings.

Our $\tilde{\Lambda}_{ab}$ differs from the Newtonian Λ_{ab} [from UCB, given in our Eq. (6d)] due to the insertion of $h^{1/2}$. This insertion is necessary for $\tilde{\Lambda}_{ab}$ to be transverse and orthogonal to f_{ab} (with respect to the background spacetime metric). The same logic leads to the introduction of the factor of $h^{1/2}$ multiplying q_{ab} in the t_Λ term in Eq. (28); it is there so that the t_Λ term is orthogonal to the t_{rr} term. We have used UCB's convention for the relative sign between the perfect fluid and shear portions of the stress-energy tensor, though we have reversed the overall sign. (However, we used the UCB convention proper in Sec. II.) The factor of $h^{1/2}$ in the coefficient of t_Λ leads to a factor of h^{-1} in the strain σ_Λ that corresponds to the von Mises breaking strain (18). We thus replace the Newtonian Eq. (17c) with

$$\sigma_\Lambda = 3\sigma_{rr}/h, \tag{30}$$

leaving Eqs. (17a) and (17b) unchanged.

One can now obtain an equation for H_0 from the perturbed Einstein equations, as in Ipser [42]. (The other two metric functions, H_2 and K, can be expressed in terms of H_0; these expressions are given by Ipser.) The concordance for notation is $\nu = 2\phi$, $e^\nu = f$, $\lambda = 2\psi$, $e^\lambda = h$, $\rho_1 = -\delta\rho$, $p_1 = -\delta p$, $\mathfrak{P}_2 = t_{rr}$, $\mathfrak{Q}_1 = h^{1/2}t_{r\perp}/\beta$, and $\mathfrak{S} = h^{1/2}t_\Lambda/\beta^2$. Additionally, Ipser's H_0 is the negative of ours. The relevant result is given in Ipser's

---

[2] Of course, this assumes that it is possible to obtain *any* symmetric tracefree tensor from the detailed relativistic expression, but—as would be expected (and can easily be seen from the expressions)—this is indeed the case, at least if one only works to first order in the perturbation, as we do here. Also, it is instructive to note that we do not need to know the specifics of the matter displacements that generate the quadrupoles we consider, only that there is a tracefree contribution to the star's stress-energy tensor whose maximum value is given by the material's shear modulus and von Mises breaking strain.

Eqs. (27)–(28), and is (in our notation)

$$H_0'' + \left(\frac{2}{r} + \phi' - \psi'\right) H_0' + \mathcal{P}(r)H_0 = 8\pi h^{1/2}\mathcal{S}(r), \quad (31)$$

where

$$\mathcal{P}(r) := 2\phi'' + 2\phi'\left(\frac{3}{r} - \phi' - \psi'\right) + \frac{2\psi'}{r} - \frac{\beta^2}{r^2}h \quad (32)$$

and

$$\begin{aligned}
\mathcal{S}(r) := &\, h^{1/2}(\delta\rho + \delta p - t_{rr}) + 2\Bigg\{(3 - r\phi')\frac{t_{r\perp}}{\beta} + r\frac{t_{r\perp}'}{\beta} \\
&+ [r^2\phi'' + r\phi'(5 - r\phi') + r\psi' - \beta^2 h/2 + 1]\frac{t_\Lambda}{\beta^2} \\
&+ r^2\phi'\frac{t_\Lambda'}{\beta^2}\Bigg\} \\
=: &\, h^{1/2}(\delta\rho + \delta p) + \mathcal{S}_{[t]}(r).
\end{aligned} \quad (33)$$

Here we have defined $\psi := (1/2)\log h$ and written $\mathcal{S}_{[t]}$ for the contributions from shear stresses. (The "$=:$" notation implies that the quantity being defined is on the right-hand side of the equality.)

We now wish to eliminate $\delta\rho$ and δp in favor of the shear stresses, as in the Newtonian calculation. We use the same projections of stress-energy conservation as in the Newtonian case (projecting onto the quantities defined by the background spacetime, for simplicity) along with the Oppenheimer-Volkov (OV) equations, giving

$$\begin{aligned}
\delta\rho + \delta p = \frac{1}{\phi'}\Bigg[&-\frac{H_0'}{2}(\rho + p) - \delta p' + t_{rr}' + \left(\frac{3}{r} + \phi'\right)t_{rr} \\
&- \frac{\beta}{r}h^{1/2}t_{r\perp}\Bigg]
\end{aligned} \quad (34)$$

and

$$\begin{aligned}
\delta p = &-\frac{H_0}{2}(\rho + p) - \frac{t_{rr}}{2} + \frac{1}{\beta h^{1/2}}[(3 + r\phi')t_{r\perp} + rt_{r\perp}'] \\
&+ h^{1/2}\left(\frac{1}{\beta^2} - \frac{1}{2}\right)t_\Lambda.
\end{aligned} \quad (35)$$

Using the second expression to substitute for $\delta p'$ in the first, we have

$$\begin{aligned}
\delta\rho + \delta p = \frac{1}{\phi'}\Bigg\{&\frac{H_0}{2}(\rho' + p') + \left[\frac{3}{r} + \phi'\right]t_{rr} + \frac{3}{2}t_{rr}' \\
&- \frac{1}{\beta h^{1/2}}\Bigg[\left(\frac{\beta^2 h}{r} + \phi' + r\phi'' - \psi'[3 + r\phi']\right)t_{r\perp} \\
&+ (4 + r[\phi' - \psi'])t_{r\perp}' + rt_{r\perp}''\Bigg] + \left(\frac{1}{2} - \frac{1}{\beta^2}\right) \\
&\times h^{1/2}(\psi' t_\Lambda + t_\Lambda')\Bigg\} \\
=: &\frac{H_0}{2\phi'}(\rho' + p') + \frac{\mathcal{S}_{[\delta\rho,\delta p]}(r)}{\phi'}.
\end{aligned} \quad (36)$$

The equation for H_0 thus becomes

$$\begin{aligned}
(\mathcal{L}_{\mathrm{GR}}H_0)(r) := &\, H_0'' + \left(\frac{2}{r} + \phi' - \psi'\right)H_0' \\
&+ \left[\mathcal{P}(r) - 4\pi h\frac{\rho' + p'}{\phi'}\right]H_0 \\
= &\, 8\pi h^{1/2}[h^{1/2}\mathcal{S}_{[\delta\rho,\delta p]}(r)/\phi' + \mathcal{S}_{[t]}(r)].
\end{aligned} \quad (37)$$

[$\mathcal{P}(r)$ and $\mathcal{S}_{[t]}(r)$ are given in Eqs. (32) and (33), respectively.] As expected, this reduces to Eq. (11) in the Newtonian limit [where we have $H_0 \to 2\delta\Phi$ and $\phi' \to g(r)$].

We now want to write the equation for H_0 in Sturm-Liouville form in order to obtain its Green function easily. To do this, we note that the appropriate "integrating factor" (for the first two terms) is $r^2(f/h)^{1/2}$, which gives

$$\begin{aligned}
[r^2(f/h)^{1/2}H_0']' + r^2(f/h)^{1/2}&\left[\mathcal{P}(r) - 4\pi h\frac{\rho' + p'}{\phi'}\right]H_0 \\
= 8\pi r^2 f^{1/2}[h^{1/2}&\mathcal{S}_{[\delta\rho,\delta p]}(r)/\phi' + \mathcal{S}_{[t]}(r)].
\end{aligned} \quad (38)$$

We also need the boundary conditions, which are given by matching H_0 onto a vacuum solution at the surface of the star. The vacuum solution that is regular at infinity is given by Eq. (20) in Hinderer [40] with $c_2 = 0$, viz.,

$$\begin{aligned}
H_0(R) = c_1\Bigg[&\left(\frac{2}{\mathcal{C}} - 1\right)\frac{\mathcal{C}^2/2 + 3\mathcal{C} - 3}{1 - \mathcal{C}} \\
&+ \frac{6}{\mathcal{C}}\left(1 - \frac{1}{\mathcal{C}}\right)\log(1 - \mathcal{C})\Bigg],
\end{aligned} \quad (39)$$

where we have evaluated this at the star's surface ($r = R$) and defined the star's compactness

$$\mathcal{C} := 2GM/Rc^2 \quad (40)$$

(now returning to showing factors of G and c explicitly). We require that H_0 and H_0' be continuous at the star's surface. The value of c_1 obtained from this matching of the internal and external solutions gives us the quadrupole moment. If we use the quadrupole moment amplitude that reduces to the UCB integral [given in our Eq. (1)] in the Newtonian limit, we have

$$Q_{22} = \frac{G^2}{c^4}\frac{M^3 c_1}{\pi}. \quad (41)$$

[This expression comes from inserting a pure $l = m = 2$ density perturbation into Eq. (2) in Hinderer [40], contracting the free indices with unit position vectors, performing the angular integral, for which the expressions in Thorne [43] are useful, and noting that the result is $(8\pi/15)Y_{22}$ times our Eq. (1). The given result then follows immediately from Hinderer's Eqs. (7), (9), and (22); we reverse the overall sign since we have reversed the UCB sign convention for the stress-energy tensor.]

We then have a Green function for Q_{22} of

$$
\begin{aligned}
\mathcal{G}_{\mathrm{GR}}(R,r) = &\left(\frac{2GM}{c^2}\right)^3 \left(1 - \frac{2GM}{Rc^2}\right)^{-1} \\
&\times \frac{\mathcal{U}(r)}{c^2 R^2 [\mathcal{U}'(R) H_0(R) - \mathcal{U}(R) H_0'(R)]}
\end{aligned}
\tag{42}
$$

(including the overall factor of $8\pi G/c^4$ that multiplies the source). Here $\mathcal{U}$ is given by $\mathcal{L}_{\mathrm{GR}}\mathcal{U} = 0$ [$\mathcal{L}_{\mathrm{GR}}$ is given in Eq. (37)], with boundary conditions $\mathcal{U}(r_0) = 1$ and $\mathcal{U}'(r_0) = 2/r_0$. [Compare Eq. (10.103) in Arfken and Weber [46], as well as our Newtonian version above.] Additionally, $H_0(R)$ and $H_0'(R)$ are given by the boundary conditions (39) with $c_1 \to 1$. [One obtains this expression by first computing the Green function for $H_0(R)$ following Arfken and Weber, then dividing through by the quantity in brackets in Eq. (39) to obtain c_1, and finally using Eq. (41) to obtain Q_{22}. We have also noted that $1/f \to h \to 1/(1 - 2GM/Rc^2)$ at the star's surface.] We thus define, for notational simplicity, two relativistic generalizations of $G_N(r)$: One,

$$
G_{\mathrm{GR}}(r) := \frac{r^2 (fh)^{1/2} \mathcal{G}_{\mathrm{GR}}(R,r)}{\phi'},
\tag{43}
$$

for the contributions from $\mathcal{S}_{[\delta\rho,\delta p]}$, and one,

$$
\bar{G}_{\mathrm{GR}}(r) := r^2 f^{1/2} \mathcal{G}_{\mathrm{GR}}(R,r),
\tag{44}
$$

for the contributions from $\mathcal{S}_{[t]}$.

With these definitions, the integral expression for the quadrupole in terms of the stresses and the structure of the background star is

$$
\begin{aligned}
Q_{22} &= \int_0^R \left[G_{\mathrm{GR}}(r) \mathcal{S}_{[\delta\rho,\delta p]}(r) + \bar{G}_{\mathrm{GR}}(r) \mathcal{S}_{[t]}(r) \right] dr \\
&= \int_0^R (\mathcal{C}_{rr} t_{rr} + \mathcal{C}_{t\perp} t_{r\perp} + \mathcal{C}_\Lambda t_\Lambda) dr,
\end{aligned}
\tag{45}
$$

where

$$
\mathcal{C}_{rr} := \left(\frac{3}{r} + \phi'\right) G_{\mathrm{GR}}(r) - \frac{3}{2} G'_{\mathrm{GR}}(r) - h^{1/2} \bar{G}_{\mathrm{GR}}(r),
\tag{46a}
$$

$$
\begin{aligned}
\mathcal{C}_{r\perp} := &-\frac{\beta h^{1/2}}{r} G_{\mathrm{GR}}(r) + \frac{2 + r(\phi' + \psi')}{\beta h^{1/2}} G'_{\mathrm{GR}}(r) \\
&- \frac{r}{\beta h^{1/2}} G''_{\mathrm{GR}}(r) + \frac{4 - 2r\phi'}{\beta} \bar{G}_{\mathrm{GR}}(r) - 2\frac{r}{\beta} \bar{G}'_{\mathrm{GR}}(r),
\end{aligned}
\tag{46b}
$$

$$
\begin{aligned}
\mathcal{C}_\Lambda := &\left(\frac{1}{\beta^2} - \frac{1}{2}\right) h^{1/2} G'_{\mathrm{GR}}(r) \\
&+ \frac{2r\phi'(3 - r\phi') + 2r\psi' - \beta^2 h + 2}{\beta^2} \bar{G}_{\mathrm{GR}}(r) \\
&- \frac{2r^2 \phi'}{\beta^2} \bar{G}'_{\mathrm{GR}}(r),
\end{aligned}
\tag{46c}
$$

and we have integrated by parts twice to obtain the second equality in Eq. (45), using the same argument as in our Newtonian calculation.

We now look at the maximum quadrupole. This is still given by the uniformly maximally strained case: We have checked numerically that the coefficients of the three stress terms are always negative for all the background stars we consider. We thus have a maximum quadrupole given by inserting Eqs. (7), (17a), (17b), and (30) into Eq. (45), yielding

$$
\frac{|Q_{22}^{\mathrm{max,GR}}|}{\bar{\sigma}_{\max}} = \sqrt{\frac{32\pi}{15}} \int_0^R \mu(r) \left\{ \left[\frac{6}{r}(h^{1/2} - 1) - 2\phi'\right] G_{\mathrm{GR}}(r) + \left[3 - \frac{r}{h^{1/2}}(\phi' + \psi')\right] G'_{\mathrm{GR}}(r) + \frac{r}{h^{1/2}} G''_{\mathrm{GR}}(r) + \mathcal{Q}^{\mathrm{stress}} \right\} dr,
\tag{47}
$$

where

$$
\mathcal{Q}^{\mathrm{stress}} := 2 \left[\frac{r\phi'(r\phi' - 3) - r\psi' - 1}{h} + r\phi' + h^{1/2} + 1\right] \bar{G}_{\mathrm{GR}}(r) + 2r\left(\frac{r\phi'}{h} + 1\right) \bar{G}'_{\mathrm{GR}}(r)
\tag{48}
$$

is the contribution from the stresses' own gravity. We have split it off both for ease of notation and because it is negligible except for the most massive and compact stars, as illustrated below. The contributions from the density and pressure perturbations are so much larger due to the factor of $1/\phi'$ present in G_{GR} [cf. Eqs. (43) and (44)]. It is easy to see that Eq. (47) reduces to Eq. (19) in the

Newtonian limit, where $h \to 1$, and we can neglect the contributions involving ϕ', ψ', and $\mathcal{Q}^{\mathrm{stress}}$.

We now show how the relations between the different maximal-strain Q_{22} Green functions [given by the integrands in Eqs. (19) and (47) without the factors of μ (but with the overall prefactor)] vary with EOS, as well as with the mass of the star for a given EOS. This gives an indica-
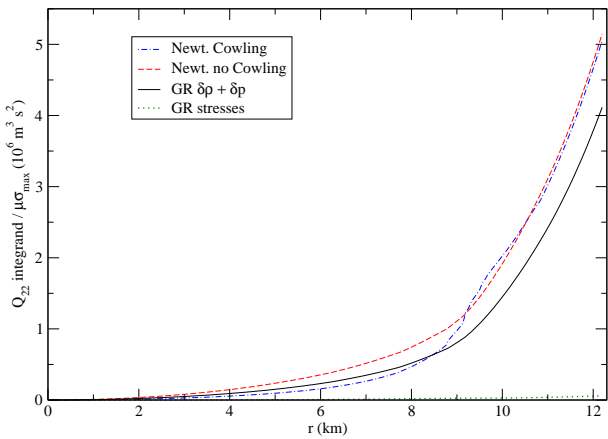
FIG. 1: The Q_{22} integrands (without the factor of $\mu\bar{\sigma}_{max}$) for the SLy EOS and an $0.500\,M_{\odot}$ star with a compactness of 0.12.

FIG. 2: The Q_{22} integrands (without the factor of $\mu\bar{\sigma}_{max}$) for the SLy EOS and a $1.40\,M_{\odot}$ star with a compactness of 0.35.
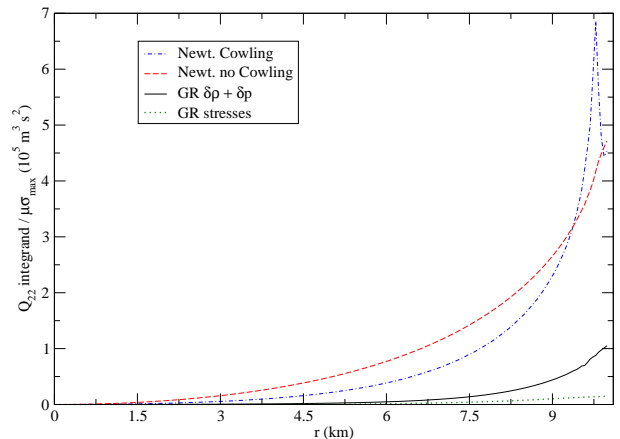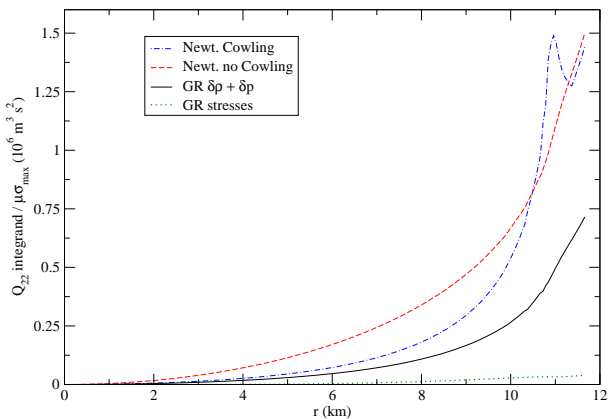

FIG. 3: The Q_{22} integrands (without the factor of $\mu\bar{\sigma}_{max}$) for the SLy EOS and a maximum mass, $2.05\,M_{\odot}$ star, with a compactness of 0.60.

FIG. 4: Ratios of the Q_{22} integrands with the Newtonian Cowling approximation integrand for the Hy1 EOS and a maximum mass, $2.06\,M_{\odot}$ star, with a compactness of 0.49. Note that the top and bottom plots have completely separate vertical axis scalings.

tion of how much difference the various approximations make in different situations. We start with the unified SLy EOS [24], obtained by Haensel and Potekhin [48] (using the table provided by the Ioffe group [49] at [50]), which is a standard choice for making predictions about crustal quadrupoles (e.g., in Horowitz [21], HJA, and our Sec. IV A). Here we illustrate the changes in the Green functions with mass for stars with masses ranging from $0.5\,M_{\odot}$ to the EOS's maximum mass of $2.05\,M_{\odot}$; see Figs. 1, 2, and 3. (All three Green functions agree extremely closely for stars around the EOS's minimum mass of $0.094\,M_{\odot}$, so we do not show this case, particularly because such low-mass neutron stars are of unclear astrophysical relevance.) These stars' compactnesses [defined in Eq. (40)] range from 0.12 to 0.6. Note that Fig. 3 has a different vertical scale than the other two plots, due to the suppression of the quadrupole for massive, compact stars (discussed below).

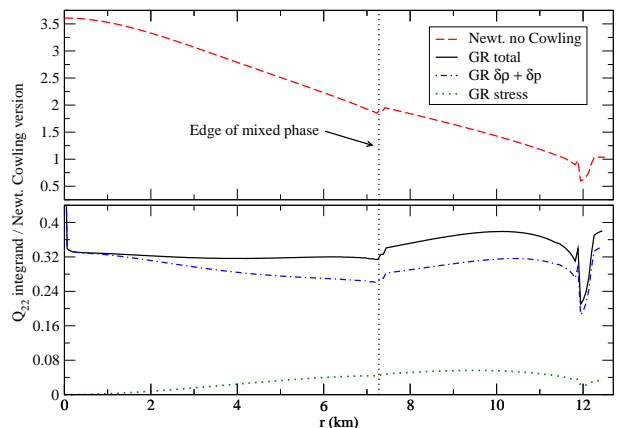We illustrate the ratios of the various Q_{22} Green func-

tions to the Newtonian Cowling approximation one for the maximum mass ($2.05\,M_{\odot}$) hybrid star using the Hy1 EOS (see Table I in [29]) in Fig. 4.[3] We see the overestimate of the Newtonian no Cowling approximation calculation for perturbations in the core, particularly com-

---

[3] As discussed in [29], for our low-density EOS, we use the same combination of the Baym, Pethick, and Sutherland (BPS) [51] EOS for $n_B < 0.001$ fm^{-3} and the Negele and Vautherin [52] EOS for 0.001 fm$^{-3} < n_B < 0.08$ fm^{-3} used by Lattimer and Prakash [53] (n_B is the baryon number density). These were obtained from the table provided by Kurkela et al. [54] at [55]. Bulk quantities of hybrid stars such as the mass and quadrupole moment (from core deformations) do not depend much on the precise choice of low-density EOS.

pared with the general relativistic (GR) version, and also see the overestimate of the Newtonian Cowling approximation version for crustal perturbations. (We do not make some sort of similar plot for the solid strange quark star case, since the expressions for the maximum quadrupole in this case end up being rather different than the integrated-by-parts ones presented in the previous sections, as we shall see in Sec. IV C.)

In all these cases, we compute the stellar background fully relativistically, using the OV equations and identifying the OV equations' Schwarzschild radial coordinate with the Newtonian radial coordinate when necessary. We have used the enthalpy form of the OV equations given by Lindblom [56] and implemented the inner boundary condition by taking the star to have an inner core of radius $r_0 = 100$ cm, whose mass is given by $(4/3)\pi r_0^3 \epsilon_0$, where ϵ_0 is the energy density corresponding to the central enthalpy that parametrizes the solution. (The spike near the origin seen in the bottom plot in Fig. 4 is due to this implementation of the inner boundary condition and has a negligible effect on the computed maximum quadrupoles.) In all cases, we have used MATHEMATICA 7's default methods to solve the differential equations, find roots, etc. We have computed as many derivatives as possible analytically, to aid numerical accuracy, e.g., using the OV equations to substitute for derivatives of the pressure, and also using the Green function equations to express second derivatives of the Green functions in terms of the functions themselves and their first derivatives.

IV. RESULTS

A. Maximum Q_{22} for crustal deformations

Here we consider the maximum quadrupoles from elastic deformations of a nonaccreted crust in three possible situations, following HJA. In particular, we use the SLy EOS (as do Horowitz [21] and HJA, though they do not refer to it by that name) and impose two comparison crustal thicknesses to ascertain how much this affects the maximum quadrupole. Here we use the same rough model for the crust's shear modulus used by HJA. We also consider the more detailed model for the shear modulus obtained using the crustal composition provided by Douchin and Haensel [24] (also used by Horowitz [21] and HJA). Here the crust's thickness is fixed to the value given in that work. In this case, we also consider a different high-density EOS that yields much less compact stars with larger crusts.

Specifically, the two comparison crustal thicknesses are given by taking the base of the crust to occur at densities of 2.1×10^{14} g cm^{-3} (thick crust, for comparison with UCB) or 1.6×10^{14} g cm^{-3} (thin crust, following a suggestion by Haensel [57]), while Douchin and Haensel place the bottom of the crust at a density of 1.28×10^{14} g cm^{-3}. For the two comparison cases, we take the shear modulus

to be 10^{16} cm^2 s^{-2} times the star's density (in g cm^{-3}). As illustrated in HJA's Fig. 2, this is an underestimate of $< 50\%$, except at the very extremes of the density range considered.[4] We plot the quadrupole moment and ellipticity for these two cases for masses between $\sim 1.2\,M_\odot$ (around the minimum observed neutron star mass—see [58]) and the SLy EOS's maximum mass of $2.05\,M_\odot$ in Fig. 5.
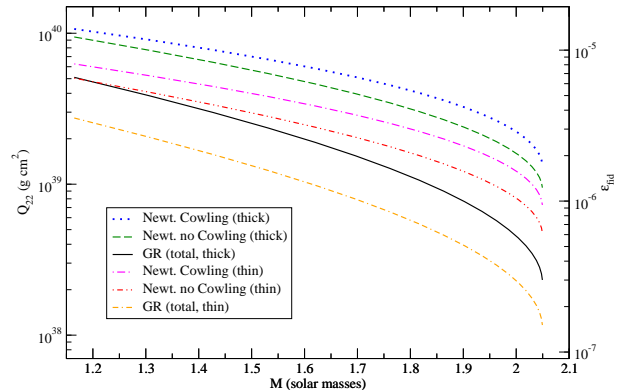
FIG. 5: The Newtonian Cowling, Newtonian no Cowling, and full relativistic (including stress contributions) values for the maximum quadrupole deformations (and fiducial ellipticity) due to crustal stresses versus mass for two choices of crustal thickness. These are computed using the SLy EOS with the rough HJA recipe for the shear modulus and a breaking strain of 0.1.

In addition to the quadrupole moments, we also show the fiducial ellipticity $\epsilon_{\rm fid} = \sqrt{8\pi/15}Q_{22}/I_{zz}$ [e.g., Eq. (2) of [12]]. Here I_{zz} is the star's principal moment of inertia, for which we use the fiducial value of $I_{zz} = 10^{38}$ kg m^2 = 10^{45} g cm^2 used in the LIGO/Virgo papers rather than the true value for a given mass and EOS, which can be greater by a factor of a few. We do this for easy comparison with the observational papers, since they frequently quote results in terms of this fiducial ellipticity instead of the quadrupole moment, which is the quantity truly measured.

Nota bene (N.B.): We present these fiducial ellipticities *only* for comparison with LIGO/Virgo results, not to give any indication of the size of the deformation. While the true ellipticity gives a measure of the size of the deformation in the Newtonian case (up to ambiguities from the fact that the true density distribution is nonuniform), it does not do so in any obvious way in the relativistic case. Nevertheless, the relativistic shape of the star's surface can be obtained from its quadrupole deformation, as

---

[4] Note that Fig. 3 in HJA is not in agreement with their Fig. 2. When we reproduce those figures, we find that the ratio μ/ρ is considerably closer to 10^{16} cm^2 s^{-2} over all the density range than the trace shown in HJA's Fig. 3, so their approximation is better than it would appear from that figure.

shown in [59]. However, if one wished to know, for instance, how much the star is deformed as a function of radius, one would need to calculate this using a detailed relativistic theory of elasticity to relate the stresses to the matter displacements, as in Penner *et al.* [60].

In the more detailed case, we use the HJA version of the Ogata and Ichimaru [25] shear modulus, combined with the Douchin and Haensel [24] results for the crust's composition. This is [correcting a typo in HJA's Eq. (20)],

$$\mu_{\text{eff}} = 0.1194 \left(\frac{4\pi}{3}\right)^{1/3} \left(\frac{1 - X_n}{A} n_b\right)^{4/3} (Ze)^2, \quad (49)$$

where X_n is the fraction of neutrons outside of nuclei, A and Z are the atomic and proton number of the nuclei, respectively, n_b is the baryon number density, and e is the fundamental charge.

Since HJA's study, there have been a few improvements to the Ogata and Ichimaru result: Horowitz and Hughto [26] have computed the effects of charge screening, finding a $\sim 7\%$ reduction in the shear modulus. Baiko [28] has also considered a relativistic model for the electron polarizability and arrived at similar conclusions. Indeed, Baiko's results suggest that screening will yield an even smaller correction in the innermost portion of the crust, where the shear modulus is the largest, and the electrons are the most relativistic, with a relativity parameter over an order of magnitude larger than the largest Baiko considers. (However, the ion charge numbers are also almost always somewhat greater than the largest Baiko considers, particularly at the very innermost portion of the crust, which will tend to increase the effect.)

Baiko [27] has also recently computed quantum corrections, and finds that they reduce the shear modulus by up to $\sim 18\%$ in some regimes. However, in our case, the reduction will be much smaller, based on the scaling of $\rho^{1/6}/(ZA^{2/3})$ given near the end of Baiko's Sec. 6. Even though our densities are over an order of magnitude greater, the nuclei we consider are also over an order of magnitude more massive than the ^{12}C composition Baiko considers, so the quantum mechanical effects end up being reduced by about an order of magnitude from the number Baiko quotes. We thus use the same Ogata and Ichimaru result used by HJA, noting that the resulting quadrupoles might be reduced by less than 10% due to charge screening and quantum effects—an error which is small compared to other uncertainties, such as crust thickness and the composition of dense matter. Indeed, there is a factor of ~ 2 uncertainty in the shear modulus due to angle averaging (even disregarding whether the implicit assumption of a polycrystalline structure for the crust is warranted): As shown by Hill [61], the Voigt average used by Ogata and Ichimaru is an upper bound on the true shear modulus of a polycrystal. A lower bound is given by the Reuss average (also discussed in Hill [61]), for which the prefactor in Eq. 49 would be 0.05106.

Note that there would be even further corrections to the shear modulus due to pasta phases (see [62]), but such phases are not present in the Douchin and Haensel model [24]. We also note that the Douchin and Haensel results only include the very innermost portion of the outer crust. However, this lack of coverage has a negligible effect on the final results for the quadrupoles, since the neglected region has at most half the radial extent of the inner crust and the shear modulus in this region is orders of magnitude below its maximum value at the bottom of the inner crust. We have checked this explicitly using the detailed calculations of the outer crust composition due to Rüster, Hempel, and Schaffner-Bielich [63], available at [64].

We plot the maximum quadrupole and ellipticity in the three approximations for the detailed shear modulus model in Fig. 6. Here we show these for the SLy EOS proper, and also for a high-density EOS that yields much less compact stars (and a crust that is ~ 2 times as thick), and thus larger maximum quadrupoles. For the latter EOS, we have chosen (for simplicity) the LKR1 hybrid EOS from [29]—the maximum compactnesses for the two EOSs are 0.60 (SLy) and 0.43 (LKR1). (We show the much larger quadrupoles that could be supported by the mixed phase in the core for the LKR1 EOS in Fig. 9, but here just show the crustal quadrupoles using the Douchin and Haensel model for the crust.)
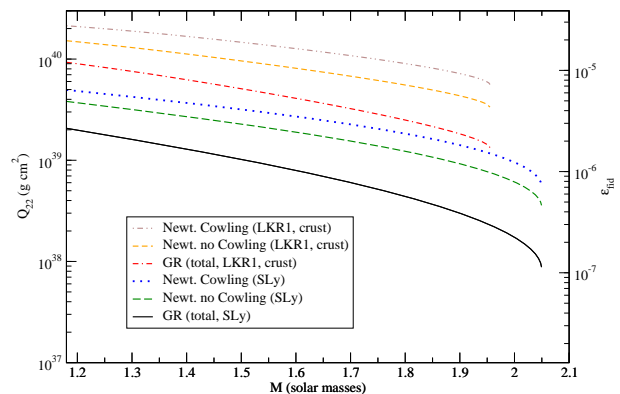

FIG. 6: The Newtonian Cowling, Newtonian no Cowling, and full relativistic (including stress contributions) values for the maximum quadrupole deformations (and fiducial ellipticity) due to crustal stresses versus mass, for the SLy EOS with the detailed Douchin and Haensel + Ogata and Ichimaru model for the shear modulus and a breaking strain of 0.1, plus the crustal quadrupoles for the LKR1 EOS with the same crustal model.

In all of these crustal results, in addition to the expected relativistic suppression of the quadrupole (which becomes quite dramatic for compact, high-mass stars), we also find that the Newtonian Cowling approximation slightly overestimates the quadrupole (by ~ 25–50%), as observed by HJA (though they found the overestimate to be considerably greater, around a factor of at least a few).

This overestimate is due to the cancellation of contributions from ρ' when one drops the Cowling approximation (see the discussion at the end of Sec. II). The overall decrease in the maximum crustal quadrupole with mass is due primarily to the fact that the crust thins by a factor of ~ 4 (SLy) or ~ 2 (LKR1) in going from a $1\,M_\odot$ star to the maximum mass star, though the quadrupole itself receives even further suppressions with mass due to relativistic effects and an increased gravitational field.

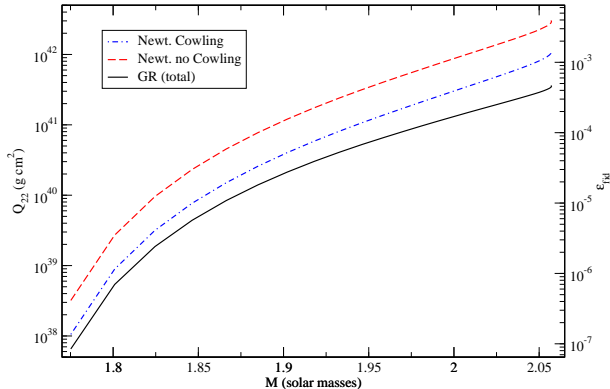## B. Maximum Q_{22} for hybrid stars

FIG. 7: The Newtonian Cowling, Newtonian no Cowling, and full relativistic (including stress contributions) values for the maximum quadrupole deformations (and fiducial ellipticity) of hybrid stars versus mass, using the Hy1 EOS with a surface tension of $\sigma = 80$ MeV fm^{-2} and a breaking strain of 0.1.

Here we display the maximum quadrupole deformations as a function of stellar mass for each of the hybrid EOS parameter sets considered in [29]. (N.B.: Most of the results from [29] we use or refer to here were corrected in the erratum to that paper.) We start by showing these values calculated in the various approximations using the Hy1 EOS (with a surface tension of $\sigma = 80$ MeV fm^{-2}; see Table I in [29]) in Fig. 7, and then restrict our attention to the relativistic results. (The relation between the results of the different approximations is roughly the same for all the hybrid EOSs we consider.) Here the maximum quadrupoles increase with mass, since the volume of mixed phase increases with mass, and this is more than enough to offset the suppressions due to relativity and the increased gravitational field.

We also show how the maximum relativistic quadrupole varies with the surface tension for the Hy1 EOS in Fig. 8. The slightly larger quadrupoles for lower surface tensions at low masses are expected, due to a slightly larger shear modulus at low pressures for lower surface tensions—see Fig. 10 in [29]. In fact, despite differences of close to an order of magnitude in the high-pressure shear modulus for the Hy1 EOS in going from a surface tension of 20 MeV fm^{-2} to one of 80 MeV fm^{-2}
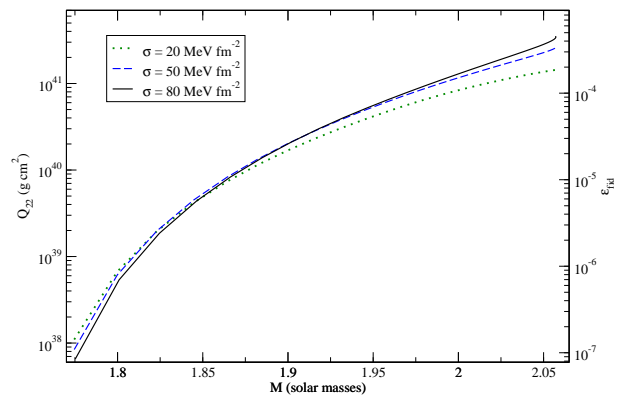

FIG. 8: The full relativistic maximum quadrupole deformations (and fiducial ellipticity) of hybrid stars versus mass, using the Hy1 EOS with various surface tensions σ and a breaking strain of 0.1.

(see Fig. 10 in [29]), the differences in the resulting maximum quadrupoles are at most a factor of a few (for large masses). This is not unexpected: These quantities are dominated by the portions of the mixed phase further out in the star, where the shear moduli have a much weaker dependence on the surface tension. (Additionally, the fact that larger surface tensions lead to smaller shear moduli at low pressures helps to minimize the effect, though the maximum quadrupoles still increase with increasing surface tension for high masses, as expected.)
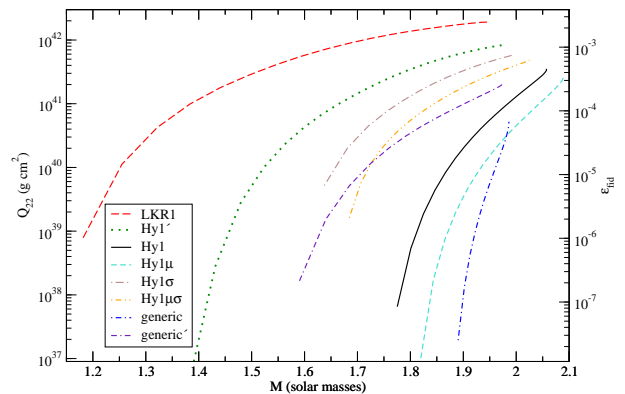
FIG. 9: The full relativistic maximum quadrupole deformations (and fiducial ellipticity) of hybrid stars versus mass, using the EOSs from Table I in [29], all with a surface tension of $\sigma = 80$ MeV fm^{-2} and a breaking strain of 0.1.

Finally, we show the maximum quadrupoles for different hybrid EOSs in Fig. 9. (Note that these curves start somewhat above the minimum masses for which the mixed phase is present, since we are mostly interested in the significantly larger maximum quadrupoles possible for larger masses.) The considerable differences are due primarily to the substantial variations in the extent of the mixed phase in stable stars with EOS param-

eters as well as the EOS dependence of the stars' compactnesses (see Table I in [29]), not to variations in the magnitude of the shear modulus for a given quark matter fraction (compared in Fig. 12 in [29]). In particular, the LKR1 EOS produces stars with a very large region of mixed phase—up to 72.5% of the star's radius—and a (relatively) small maximum compactness—only 0.433. (Note that our quadrupole curve for the LKR1 EOS ends slightly short of the EOS's maximum mass of $1.955\,M_\odot$, only going to $1.948\,M_\odot$, due to problems with the numerics.)

N.B.: These maximum quadrupoles may all be overly optimistic. First, as was discussed in Sec. IV A, the averaging used to obtain the effective shear modulus only gives an upper bound on the true shear modulus of a polycrystal. (We do not quote results for the Reuss lower bound here, since it is only straightforward to obtain for the three-dimensional droplet phases. However, we shall note that preliminary investigations, using the Reuss bound for the droplet phases, and the Voigt bound for the rest, give reductions in the maximum quadrupoles of up to ~ 5 for lower masses.)

Second, the relatively large value we have chosen for the surface tension also increases the maximum quadrupoles, while recent calculations place the surface tension on the low side ($\sim$ 10–30 MeV fm^{-2})—see [65] for the latest results. Nevertheless, as we show in the Appendix, the mixed phase is nevertheless favored by global energy arguments even for these large surface tensions. The maximum quadrupoles are also affected by the method of EOS interpolation and the lattice contributions to the EOS, as is illustrated in the Appendix, though the largest change is only $\sim 40\%$ (at least for the LKR1 and Hy1$'$ EOSs, the two EOSs that yield the largest quadrupoles).

Note that LIGO's current upper limits on fiducial ellipticity in the most interesting cases (the Crab pulsar, PSR J0537–6910, and Cas A) [6, 7] are $\sim 10^{-4}$, corresponding to a quadrupole moment of $\sim 10^{41}$ g cm^2. The first hybrid star estimate by Owen [12] was an order of magnitude lower. Thus our new results here show that current LIGO upper limits are interesting not only for quark stars but also for hybrid stars, at least high-mass ones. Indeed, the most extreme case we consider, the LKR1 EOS with high surface tensions, gives maximum quadrupoles of a few $\times 10^{42}$ g cm^2, which are above and therefore relevant to the limits set by Virgo for the Vela pulsar [8].

C. Maximum Q_{22} for crystalline color superconducting quark stars

Here we consider stars made of crystalline color superconducting quark matter, for which the shear modulus has been estimated by Mannarelli, Rajagopal, and

Sharma [30].[5] [See Eq. (1) in Haskell *et al.* [23] for the expression in cgs units.] Such stars have also been treated (with varying degrees of sophistication) by Haskell *et al.* [23], Lin [19], and Knippel and Sedrakian [20]. However, only Lin considers the case of a solid quark star, as we will do here, and does so using quite a rough model. (The others consider crystalline color superconducting cores in hybrid stars.)

Since strange quark stars have a nonzero surface density—and solid quark stars have a nonzero surface shear modulus, with the standard density-independent treatment of the superconducting gap—we have to make some changes to our previously obtained expressions in order to treat them.

First, the outer boundary condition changes. The potential (in the Newtonian case) and metric perturbation (in the GR case) are no longer continuous at the star's surface, due to the presence of ρ' in both equations [see Eqs. (12) and (38)]. As discussed in Hinderer *et al.* [66] (following Damour and Nagar [67]), one can obtain the distributional contribution to the boundary conditions [Eqs. (13) and (39)] using the usual procedure of integrating the defining differential equation over $[R - \epsilon, R + \epsilon]$ and taking the limit $\epsilon \searrow 0$. In the Newtonian case, this gives [defining ρ_- as the density immediately inside the star's surface and R^- to mean evaluation at $R - \epsilon$ in the limit $\epsilon \searrow 0$]

$$\delta\Phi'(R^-) = \left[\frac{4\pi G}{g(R)}\rho_- - \frac{3}{R}\right]\delta\Phi(R), \qquad (50)$$

and in the GR case, we have (with $G = 1$)

$$H_0'(R^-) = H_{0,\text{old}}'(R) + \frac{4\pi h}{\phi'(R)}\rho_- H_0(R), \qquad (51)$$

where $H_{0,\text{old}}'(R)$ is computed using Eq. (39). We thus make the replacement $3RF(R) \rightarrow [3 - 4\pi G\rho_- R/g(R)]RF(R)$ in the expression for the Newtonian Green function [Eq. (23)], and the replacement $H_0'(R) \rightarrow H_{0,\text{old}}'(R) + 4\pi h\rho_- H_0(R)/\phi'(R)$ in the GR case [Eq. (42)]. These changes in the boundary conditions increase the maximum quadrupole by a factor of $\lesssim 2$ in the example case considered below; the largest effect is for the least massive stars considered.

Second, we would have to keep the boundary terms at the outer boundary when integrating by parts to obtain the expressions for the maximum quadrupole, since the shear modulus no longer vanishes at the star's surface. However, since here the shear modulus is smooth, it is numerically preferable not to perform any integration by parts, thus avoiding potential problems with large cancellations between the surface and integrated terms. In

---

[5] This estimate is not angle averaged, but Mannarelli, Rajagopal, and Sharma's calculation has relatively large uncontrolled remainders, so we do not worry about the effects of angle averaging here.

this case, the expressions for the quadrupole assuming the UCB maximum uniform strain are [cf. Eqs. (19) and (47)]

$$\frac{|Q_{22}^{\text{UCB strain},N}|}{\bar{\sigma}_{\max}} = \sqrt{\frac{32\pi}{15}} \int_0^R G_N(r)[r\mu''(r) - \mu'(r)]dr \tag{52}$$

and

$$\frac{|Q_{22}^{\text{UCB strain, GR}}|}{\bar{\sigma}_{\max}} = \sqrt{\frac{32\pi}{15}} \int_0^R \big[G_{\text{GR}}(r)\mathcal{I}_{[\delta\rho,\delta p]}^{\text{UCB}}(r) \\ + \bar{G}_{\text{GR}}(r)\mathcal{I}_{[t]}^{\text{UCB}}(r) \big] dr, \tag{53}$$

where

$$\mathcal{I}_{[\delta\rho,\delta p]}^{\text{UCB}}(r) := \left[\frac{6}{r}(h^{1/2}-1) - 2\phi' + \frac{r\phi'' + \phi'(1-r\psi') - \psi'}{h^{1/2}} \right] \mu(r) + \left[\frac{2 + r(\phi'-\psi')}{h^{1/2}} - 3 \right] \mu'(r) + \frac{r\mu''(r)}{h^{1/2}}, \tag{54a}$$

$$\mathcal{I}_{[t]}^{\text{UCB}}(r) := 2\left\{ \frac{r\phi'[r(\phi'+2\psi')-5] - r\psi' - r^2\phi'' - 1}{h} + r\phi' + h^{1/2} \right\} \mu(r) - 2r\left(\frac{r\phi'}{h} + 1 \right)\mu'(r). \tag{54b}$$

However, these expressions will not actually yield the maximum quadrupole in this case, due to an important difference between the cases where the shear modulus vanishes at the star's surface and those where it does not. It is simplest to see this in the Newtonian case for a star with a constant shear modulus: Since the UCB maximum strain expression (52) only depends upon derivatives of the shear modulus, it predicts a *zero* maximum quadrupole, which seems absurd. One can, however, make a small adjustment to the form of the maximum strain one considers to yield a nonzero quadrupole in this case. This modification will also yield considerably larger maxima in the realistic case we consider, as well, where the shear modulus is close to constant—it decreases by less than a factor of 2 in going from the star's center to its surface in the example case we consider below.

Specifically, in the case of a slowly varying shear modulus, with $\mu(r) \gg |r\mu'(r)|, |r^2\mu''(r)|$, appropriate for strange quark stars, we want the terms involving μ itself to be largest. The appropriate choice for the strain in this case is most readily apparent from inspection of the Newtonian expression for the maximum quadrupole in terms of the stress tensor components, Eq. (15). We want the maximum contribution from the undifferentiated terms, which implies that we want t_{rr} and $-t_{r\perp}$

to be as large as possible. For t_Λ, we note that since $\mu'(r) < 0$, we also want $-t_\Lambda$ to be as large as possible. Realizing that we can freely change the sign of any of the $\sigma_\bullet$ that give maximum uniform strain [given for the Newtonian case in Eqs. (17); cf. Eq. (65) in UCB], we thus reverse the sign of $\sigma_{r\perp}$ and σ_Λ. [The same logic holds for the more involved GR case, as well, where the appropriate expression for σ_Λ will be the negative of Eq. (30).]

The resulting expressions for the putative maximum quadrupole in this case are thus

$$\frac{|Q_{22}^{\text{mod. strain},N}|}{\bar{\sigma}_{\max}} = \sqrt{\frac{32\pi}{15}} \int_0^R G_N(r)\left[\frac{12}{r}\mu(r) + 5\mu'(r) \\ + r\mu''(r) \right] dr \tag{55}$$

and

$$\frac{|Q_{22}^{\text{mod. strain, GR}}|}{\bar{\sigma}_{\max}} = \sqrt{\frac{32\pi}{15}} \int_0^R \big[G_{\text{GR}}(r)\mathcal{I}_{[\delta\rho,\delta p]}^{\text{mod}}(r) \\ + \bar{G}_{\text{GR}}(r)\mathcal{I}_{[t]}^{\text{mod}}(r) \big] dr, \tag{56}$$

where

$$\mathcal{I}_{[\delta\rho,\delta p]}^{\text{mod}}(r) := \left[\frac{6}{r}(h^{1/2}+1) + 2\phi' + \frac{r\phi'' + \phi'(1-r\psi') - \psi'}{h^{1/2}} \right] \mu(r) + \left[\frac{2 + r(\phi'-\psi')}{h^{1/2}} + 3 \right] \mu'(r) + \frac{r\mu''(r)}{h^{1/2}}, \tag{57a}$$

$$\mathcal{I}_{[t]}^{\text{mod}}(r) := -2\left\{ \frac{r\phi'[5 - r(\phi'+2\psi')] + r\psi' + r^2\phi'' + 1}{h} - r\phi' + h^{1/2} \right\} \mu(r) - 2r\left(\frac{r\phi'}{h} + 1 \right)\mu'(r). \tag{57b}$$

In principle, these merely give a lower bound on the max-

imum quadrupole, unlike the case in which the shear

modulus vanishes below the surface, where there is a firm argument that maximum uniform strain maximizes the quadrupole. However, even if they do not give the absolute maximum, they should be quite close for cases like the one we consider here, where the shear modulus varies quite slowly.
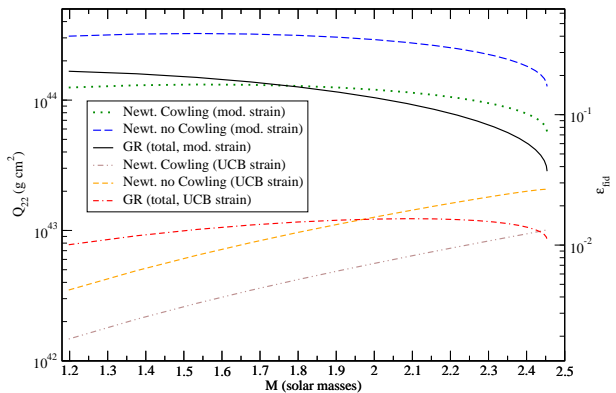

FIG. 10: The Newtonian Cowling, Newtonian no Cowling, and full relativistic (including stress contributions) values for the quadrupole deformations (and fiducial ellipticity) of maximally strained strange quark stars versus mass, using the EOS discussed in the text with a breaking strain of 0.1. We show these both for the standard UCB uniform maximum strain, and our modification that yields significantly larger quadrupoles in this case.

Applying these expressions to a specific case, we use the strange quark matter EOS calculated by Kurkela, Romatschke, and Vuorinen (KRV) [31], generating an EOS for the parameter values of interest using the MATHEMATICA notebooks available at [68]. The relevant parameters are the values of the $\overline{\text{MS}}$ renormalization point, $\Lambda_{\overline{\text{MS}}}$, and the strange quark mass, m_s, both at a scale of 2 GeV, along with the coefficient in the relation between the renormalization scale and the quark chemical potential, X, the color superconductivity gap parameter, Δ (taken to be independent of density),[6] and the minimal quark chemical potential at which strange quark matter

exists, $\mu_{q,\min}$. We consider the EOS obtained by choosing $\Lambda_{\overline{\text{MS}}} = 355$ MeV, $m_s = 70$ MeV, $X = 4$, $\Delta = 10$ MeV, and $\mu_{q,\min} = 280$ MeV. This parameter set yields a maximum mass of $2.45\,M_\odot$, with a maximum compactness of 0.467.

These parameter choices were generally inspired by those considered at [68], though with a smaller value of Δ, to place us well within the crystalline superconducting regime. However, as Knippel and Sedrakian [20] suggest, the crystalline phase could still be favored for considerably larger Δs, up to ~ 100 MeV, for the low-temperature case relevant for neutron stars. We thus note that increasing Δ decreases the maximum mass, and increases the maximum quadrupole, though the latter is increased by considerably less than the naïve scaling of Δ^2 one would expect from the scaling of the shear modulus, likely due to the increased compactness of the stars with larger Δs: For $\Delta = 100$ MeV, we have a maximum mass and compactness of $2.12\,M_\odot$ and 0.508, respectively, and a maximum quadrupole of $\sim 3.5 \times 10^{45}$ g cm^2 for a $1.4\,M_\odot$ star, ~ 20 times that for $\Delta = 10$ MeV. However, one must bear in mind that our perturbative treatment starts to become questionable with such large gap parameters, for which the maximum shear stresses are more than 10% of the background's energy density. The uncontrolled remainders in the Mannarelli, Rajagopal, and Sharma [30] calculation of the shear modulus also increase as the gap parameter increases.

We show the quadrupole for a maximally uniformly strained star in the three approximations (Newtonian Cowling, Newtonian no Cowling, and GR) for both the UCB and modified maximum strain choices for this EOS in Fig. 10. Here we have used a breaking strain of 0.1, by the same high pressure argument as in the mixed phase case. (While the very outermost portions of the star are at low pressure, the parts that are at a lower pressure than the crustal case for which the 0.1 breaking strain was calculated make negligible contributions to the quadrupole.)

N.B.: To obtain the EOS used for this figure, we made some slight modifications to the KRV EoScalc MATHEMATICA notebook so that it would output particle number densities on a denser mesh for low strange quark chemical potentials. This then gave an EOS table with better low-pressure coverage than their default settings produced. We still needed to perform an extrapolation of the EOS to zero pressure, where we found that a linear extrapolation of the energy density and quark chemical potential in terms of the pressure using the lowest two entries of the table provided a good fit. (More involved approaches involving fitting to more points and/or a quadratic extrapolation produce very similar results.)

Additionally, it is worth pointing out that the applying the KRV results to compact stars pushes their second-order perturbative calculation towards the edge of its domain of validity. However, in our case, the smallest value of the quantum chromodynamics (QCD) renormalization scale we consider is 1.12 GeV, at which value the

---

[6] Note that Δ enters the KRV EOS through a color flavor locked (CFL) pressure term. This is not quite appropriate for the crystalline color superconducting phase we consider here, since it assumes that all the quarks pair, while only some of them pair in the crystalline phase. However, as discussed in Sec. VI B of [69], the condensation energy of the crystalline phases is easily $1/3$ to $1/2$ that of the CFL phase with zero strange quark mass, which is the pressure contribution used by KRV. We have thus not altered this term in our calculations, since the contribution is already approximate, in that it assumes a density-independent gap parameter. Moreover, we only consider a fairly low value of Δ, while Knippel and Sedrakian [20] suggest that the crystalline phase might be favored up to $\Delta = 100$ MeV. Our EOS may thus simply correspond to a slightly larger value of Δ, which would increase the maximum quadrupole, since the shear modulus scales as Δ^2.

QCD coupling constant is ~ 0.45. Thus, the uncontrolled remainders in the expansion are suppressed by at least a factor of ~ 0.1. (While Rajagopal and Shuster [70] find that perturbative QCD calculations of the color superconducting gap are only reliable at energy scales of $\gtrsim 10^5$ GeV, the specifics of this calculation are rather different from the calculation of the EOS we are considering here, where the gap is taken as an input parameter.) While it is unreasonable to expect this calculation to be a truly accurate description of strange quark matter, it is not clear that any of the alternative descriptions of strange quark matter are *a priori* guaranteed to be a better description of the physics, given the very considerable uncertainties associated with this phase of matter.

V. DISCUSSION

Previous studies of the tidal and magnetic deformations of compact stars have found similar relativistic suppressions of quadrupole moments with compactness. In the tidal case, see the Love number computations in [40, 66, 67, 71, 72]. In the case of magnetic deformations, the expected suppressions are seen in, e.g., [13–16]. In fact, since the largest compactness considered in these latter papers is only 0.48 (in [13]), one imagines that they overestimate the maximum quadrupoles by at least a factor of a few for more compact stars (for a fixed magnitude of magnetic field).

As was argued by Damour and Nagar [67] in the tidal case, all these suppressions are primarily related to the "no-hair" property of black holes: The largest relativistic suppression we find comes from the boundary conditions [through the $H_0(R)$ and $H_0'(R)$ in the Green function's denominator—see Eq. (42)], where one matches on to the external vacuum spacetime. For instance, for the SLy EOS's maximum compactness of 0.6, $H_0(R)$ and $H_0'(R)$ are ~ 3.5 and ~ 6 times their Newtonian values [which can be obtained from the first term of Eq. (21) in Hinderer [40]]. In fact, these ratios go to infinity in the formal black hole limit, where the compactness approaches unity, as required by the no-hair property, and discussed by Damour and Nagar [67] (see their Secs. IV C and VII A, but note that their definition for the compactness is half of ours). This implies that the stiffness of spherically symmetric curved vacuum spacetime suppresses the quadrupole. The quadrupole is also suppressed by a larger effective gravitational acceleration (given by ϕ'), which appears in the denominator of G_{GR}, replacing the Newtonian $g(r)$ [cf. Eqs. (14) and (43)]. (But recall that we always compute the background stellar structure relativistically, so this larger acceleration *only* affects the perturbation equations, and not, e.g., the thickness of the crust for a given mass and EOS, which is the same in both the Newtonian and relativistic calculations of the quadrupole.)

Our results imply that nearly all of the Newtonian computations of quadrupoles due to elastic deformations of relativistic stars overestimate the quadrupole moment, often by at least a factor of a few. The only exceptions we have found are for low-to-mid mass strange quark stars and for elastic stresses in the cores of neutron stars around $0.5\,M_\odot$. In both of these cases, the Newtonian Cowling approximation is a slight underestimate for contributions to the quadrupole, though the Newtonian no Cowling version is still an overestimate. See Fig. 1 for an illustration in the core case; but note that neutron stars with such low masses are not known to exist in nature. The overestimate from performing a Newtonian Cowling approximation calculation can be ~ 6 for massive stars whose quadrupole is being generated by an elastic deformation near the crust-core interface, as considered by UCB and others. This is due in part to the sudden changes in density at that interface entering directly through g'', as discussed at the end of Sec. II.

However, the calculations by Horowitz [21] for crustal deformations of very low mass stars only receive negligible corrections (of $\lesssim 5\%$), since he considers compactnesses of ~ 0.01. In fact, one makes even smaller errors in using the Cowling approximation to treat these stars, since the changes in density in the crust (times $4\pi G r^2$) are much smaller than the star's gravitational field there.

No neutron stars with such low masses have ever been observed (nor is there a compelling mechanism for forming them). Nevertheless, Horowitz remarks that gravitational wave detection of gravitational waves from elastically deformed neutron stars will, *ceteris paribus*, be biased towards low(er) mass neutron stars, if one considers deformations generated by crustal stresses. This is an important point, particularly when considering the astronomical interpretation of detections (or even upper limits), and the results we present here make the bias against high-mass stars even stronger. (This bias also applies to solid quark stars, though there it is rather weak. It does *not* apply to hybrid stars, however, where it is high-mass stars that can sustain the largest quadrupoles.)

Of course, one must remember that all of these values are maxima, assuming a maximally strained star, while there is no reason, *a priori*, for a given star to be maximally strained. Moreover, as UCB and HJA note, these calculations assume that all the strain goes into the $l = m = 2$ perturbation, though strain in other modes (e.g., the $l = 2$, $m = 0$ mode due to rotation) can push the lattice closer to its breaking strain while not increasing the $l = m = 2$ quadrupole.

VI. CONCLUSIONS AND OUTLOOK

We have presented a method for calculating the maximum elastic quadrupole deformation of a relativistic star with a known shear modulus and breaking strain. We then applied this method to stars whose elastic deformations are supported by a shear modulus either from the Coulomb lattice of nuclei in the crust, a hadron–quark mixed phase in the core, or crystalline superconducting

strange quark matter throughout the star. (In the last case, we have made the requisite changes to the method so that it is valid when the star has a nonzero surface density and the shear modulus does not vanish at the star's surface.) In all but the strange quark case, we find that the relativistic quadrupole is suppressed, compared with the standard, Newtonian Cowling approximation calculation of the quadrupole, at least for stars with masses of $\gtrsim 1\,M_\odot$ (corresponding to the observed masses of neutron stars) and the EOSs we have investigated. These suppressions can be up to ~ 4 in the hybrid case, and ~ 6 in the crustal case. In the strange quark star case, the Newtonian Cowling approximation calculation slightly underestimates the quadrupole (by tens of percent) for low-to-standard mass stars, but is still an overestimate of ~ 2 at higher masses.

These suppressions strengthen the Horowitz [21] argument that searches for gravitational waves from elastically deformed neutron stars supported by crustal stresses are biased towards lower-mass stars. The same argument also applies to strange quark stars, though there the suppressions with increasing mass are less severe (and the maximum quadrupoles are all considerably larger). However, this argument does not apply to quadrupole deformations of hybrid stars, since the increase in the size of the region of mixed phase with increasing mass dominates the various suppressions.

Our results also imply that many of the previous calculations of elastic quadrupoles (e.g., [18–20, 22, 23]) will need their results revised downwards. (While we find much larger maximum quadrupoles for solid strange quark stars than did Lin [19], this is only because we assume a breaking strain 10 times that assumed by Lin. If we take the same 10^{-2} breaking strain as does Lin, then we find a suppression of a factor of a few, though this is very likely within the uncertainties of Lin's calculation, which assumed a uniform density, incompressible star with a uniform shear modulus.)

It is instructive to compare our results with the numbers quoted in Pitkin's review [10]. All of these were obtained by Pitkin using scalings given in the aforementioned papers, sometimes updating to the Horowitz and Kadau [32] breaking strain, and provide a good overview of the standard Newtonian predictions. None of our detailed calculations for maximum crustal quadrupoles approach the high values Pitkin obtained using UCB's fitting formula (as corrected by Owen [12]). However, our very largest hybrid star quadrupoles are an order of magnitude above Pitkin's quoted maximum, even if one only assumes a breaking strain of 10^{-2}, as does Pitkin. Additionally, our estimates for maximum solid quark star quadrupoles ($\sim 10^{44}$ g cm^2 for $1.4\,M_\odot$ stars) are considerably larger than the ones quoted by Pitkin (based on a different shear modulus model), even if we reduce them by an order of magnitude due to scaling the breaking strain to Pitkin's 10^{-2}. In fact, they are in the same range as those Pitkin quotes for a model for crystalline superconducting hybrid stars (with an optimistic gap pa-

rameter 5 times the one we used for solid quark stars, leading to a shear modulus ~ 40 times our shear modulus's maximum value).

Even with the relativistic suppressions, we obtain maximum quadrupole deformations of a few $\times\ 10^{42}$ g cm^2 in the hybrid case for a very stiff hadronic EOS, and a few $\times\ 10^{41}$ g cm^2 for more realistic cases. In both situations, the largest maximum quadrupoles are given by the most massive stars. These values are proportional to the breaking strain and assume that the Horowitz and Kadau [32] breaking strain of about 0.1 is applicable to the mixed phase. Such large quadrupole deformations were previously thought only to be possible for solid quark stars (see [12, 19, 20, 23]), or from crustal deformations in the very low-mass neutron stars considered by Horowitz [21]. These large deformations (corresponding to fiducial ellipticities of a few $\times\ 10^{-3}$ in the extreme case, and $\sim 5 \times 10^{-4}$ in a more realistic case) would be able to be detected by current LIGO searches for gravitational waves from certain known neutron stars [6–8]. (However, we must note that there is no reason to assume that such isolated stars are anywhere near maximally strained, even neglecting the uncertainties in the description of their interiors.)

The prospects for crustal quadrupoles are now somewhat less optimistic, and definitely favor lower-mass stars. However, for a canonical $1.4\,M_\odot$ neutron star, we find that the maximum relativistic crustal quadrupole is in the range $\sim (1\text{–}6) \times 10^{39}$ g cm^2 [corresponding to fiducial ellipticities of $\sim (1\text{–}8) \times 10^{-6}$], depending on the model used for the crust and the high-density EOS. (Note that the fully consistent Douchin and Haensel model with its associated high-density EOS yields the lowest numbers. Additionally, there is the possibility of a further reduction of up to ~ 2 due to the angle averaging procedure used to obtain the shear modulus.) On the high side, these numbers are consistent with those given previously for breaking strains of 0.1 by Horowitz [21, 32],[7] though they are a factor of ~ 5 lower than the maximum Pitkin [10] obtained using scalings of previous results and the maximum value given by HJA (scaled to this breaking strain). For stars around $2\,M_\odot$, the relativistic suppressions lead to maximum quadrupoles that are nearly an order of magnitude smaller than those for a $1.4\,M_\odot$ star in the compact SLy case: $\sim (1\text{–}5)\times 10^{38}$ g cm^2 [corresponding to fiducial ellipticities of $\sim (1\text{–}6) \times 10^{-7}$]; and even in the much less compact LKR1 case, there is a suppression of ~ 5. Previous Newtonian studies (see Fig. 3 in [21])

---

[7] But recall that the results from Horowitz [21] were obtained using the SLy EOS and crustal composition results, so they are the same as our Newtonian Cowling approximation SLy predictions, given in Fig. 6, except $\sim 7\%$ lower, since Horowitz is using the Horowitz and Hughto [26] result for the shear modulus. In the fully relativistic case, one requires a thicker crust than provided by the pure SLy results to obtain values for the maximum quadrupole comparable to those given by Horowitz.

had only found suppressions of around a factor of 4, due to the thinning of the crust and the increase in Newtonian gravity with increasing mass. It will be interesting to consider further models for the crustal composition and EOS in this case, particularly the large suite of crustal models including the pasta phases recently calculated by Newton, Gearheart, and Li [73]. (See [74] for order-of-magnitude estimates of the maximum quadrupole for these models, illustrating the sensitive dependence on the slope of the symmetry energy.)

One can also compare these maximum elastic quadrupoles with those generated by an internal magnetic field. Here the values depend, of course, upon the equation of state, compactness, and—perhaps most crucially—magnetic field topology, as well as the quantity one chooses to use to measure the magnitude of the magnetic field. But sticking to order-of-magnitude numbers, and considering a canonical $1.4\,M_\odot$ neutron star, Frieben and Rezzolla [16] show that a toroidal internal field of $\sim 10^{15}$ G would generate a quadrupole of $\sim 10^{39}$–10^{40} g cm^2, comparable to the maxima we find for crustal quadrupoles. Similarly, quadrupoles of $\sim 10^{41}$–10^{42} g cm^2, around the maxima we find for hybrid stars, could come from magnetic fields of $\sim 10^{16}$ G, while the maximum quadrupoles of $\sim 10^{44}$ g cm^2 we find for crystalline strange quark stars could also be generated by magnetic fields of $\sim 10^{17}$ G, close to the maximum allowed field strength. (But note that these magnetic deformations are all computed for ordinary, purely hadronic neutron stars. Additionally, the quoted maximum elastic quadrupoles in the hybrid case are attained only for more massive stars than the $1.4\,M_\odot$ stars for which we are quoting the magnetic deformation results.) The quoted values for magnetic quadrupoles come from the fits given in Sec. 7 of Frieben and Rezzolla [16], except for the final ones, which are obtained from inspection of their Fig. 5 and Table 3. All these values agree in order of magnitude with the predictions for the twisted torus topology given by Ciolfi, Ferrari, and Gualtieri [14], and with many other studies for various topologies cited in Frieben and Rezzolla [16]. But note that very recent calculations by Ciolfi and Rezzolla [17] show that the magnetic field required to obtain a given quadrupole deformation with the twisted torus topology could be reduced by about an order of magnitude if the toroidal contribution dominates.

One would also like to make relativistic calculations of the maximum energy that could be stored in an elastic deformation. This would be useful in properly computing the available energy for magnetar flares, for instance. (Using Newtonian scalings, Corsi and Owen [75] estimated that the hybrid case was especially interesting compared to existing LIGO upper limits for gravitational wave emission from such flares.) The basic expressions (at least in the perfect fluid case) appear to be readily available in the literature (see, e.g., [76, 77]; [37, 78] give related results including elasticity). However, one cannot apply these directly to the crustal and hybrid cases, even in the Newtonian limit, due to the distributional

nature of the density and pressure perturbations. Specifically, the sudden change in shear modulus at the phase transitions gives delta functions in the derivatives of the density and pressure perturbations. Since the energy expressions involve squares of these derivatives, one would have to invoke some sort of regularization procedure, or apply a different method. Developing appropriate expressions for this case will be the subject of future work.

Returning to the quadrupoles, one might also want to consider the shape of the deformed star, particularly in the relativistic case—the ellipticity is already only a rough indicator of the shape of the deformation in the Newtonian case—as has now been done in [59]. But the effects of the star's magnetic field are surely the most interesting to consider, from its influence on the lattices that support elastic deformations, to the changes to the boundary conditions at the star's surface from an external magnetic field (particularly for magnetars), to the internal magnetic field's own contribution to the star's deformation. One might also want to consider the lattice's full elastic modulus tensor in this case, instead of simply assuming a polycrystalline structure and angle averaging to obtain an effective isotropic shear modulus, as was done here. (And even if one assumes a polycrystalline structure, one could use more involved, sharper bounds on the shear modulus than the ones considered here—see [79] for a classic review of such bounds.)

Appendix: Hadron–quark hybrid stars and the binding energy argument

As we mentioned in Sec. II C of [29], if the surface tension is large enough, the mixed phase is not locally favored energetically (i.e., at a fixed baryon density), compared to the individual pure phases. (This was first noted by Heiselberg, Pethick, and Staubo [80] and later discussed by Alford *et al.* [81].) However, as was also noted in [29], the entire region of mixed phase can still be favored due to global energy arguments, especially when one considers the binding energy of the star (for a fixed total baryon number): One expects the stars with the largest binding energy (i.e., smallest gravitational mass) for a given total baryon number to be favored. In this calculation, we always compare with a purely hadronic star. One would expect the Maxwell construction case with a sharp interface between the two phases to produce more strongly bound stars than the purely hadronic case, given the local energy results presented in [80, 81]. However, at

least for the EOSs we consider, the Maxwell construction stars with total baryon numbers up to the total baryon number of the corresponding maximum mass hybrid star only contain hadronic matter.

Specifically, if we compute the gravitational mass of a hybrid star with a given total baryon number, we find that this mass is smaller (corresponding to a larger binding energy) than that of a purely hadronic star constructed with the same hadronic EOS parameters as the hybrid EOS. However, these mass differences are not very large, only $\sim 0.006 \, M_\odot$ in the most extreme case (the most massive stars with the LKR1 EOS), and usually considerably smaller. One thus might be concerned that this conclusion could be reversed if one includes the contributions of the lattice to the EOS, viz., the lattice's energy density and pressure, and the contributions of the surface tension to the energy density (through the cell energy). Nevertheless, we find that this is not the case.

Indeed, we find that the mixed phase is favored by the binding energy argument for all the EOS parameters we consider, even for a surface tension as large as $\sigma = 80$ MeV fm^{-2}, more than twice as large as the surface tensions favored by recent calculations [65], and large enough that the mixed phase is not locally energetically favored. In fact, for these surface tensions, the mixed phase stars with the additions to the EOS from the blobs and lattice energy are even more strongly favored by the binding energy argument than those with no additions. Of course, as we mentioned in [29], the computations of the lattice additions to the EOS have some uncertainty, in particular due to our approximate treatment of charge screening. However, we do not expect this to change the qualitative results from the binding energy argument, since that the changes in the binding energy from including the lattice and blob contributions to the energy are relatively small ($\lesssim 10\%$). Moreover, we expect that more accurate computations of the cell and lattice energy would reduce their contributions. Indeed, Christiansen and Glendenning [82, 83] argue that the mixed phase should *always* be favored, and any calculation that predicts otherwise must be incomplete or using inapplicable input parameters.

We now describe the specifics of the binding energy calculation. We calculate the mass differences by first computing the total baryon number as a function of mass for the purely hadronic stars and then using bisection to locate the hybrid star with the same total baryon number. However, as noted by Haensel and Prószyński [84], the standard method of logarithmic interpolation of an EOS table is insufficiently accurate to allow one to compute the gravitational masses and baryon numbers with the accuracy we need. One must, instead, use a thermodynamically consistent method of interpolation—i.e., one for which the first law of thermodynamics is satisfied exactly. And, indeed, if we use the standard logarithmic interpolation, we find that the additions to the EOS have a much larger effect on the binding energy differences, and the mixed phase is only favored by the binding

energy argument for higher masses, if at all.

Haensel and Prószyński [84] provide such a thermodynamically consistent method of interpolation in their Sec. IIc, which we use to perform the binding energy calculation. There is an alternative expression for the baryon number density as a function of radius given in Eq. (6) of Haensel and Potekhin [48] (also obtained using the first law of thermodynamics), but we find the Haensel-Prószyński interpolation to be preferable, in our experiments. Specifically, we have checked that our qualitative conclusions remain unchanged if use the EOS output on a finer mesh of baryon number densities (with half the spacing of the original mesh) and have found that the results of the Haensel-Prószyński interpolation are less sensitive to changes in the mesh on which the EOS table is output than the Haensel-Potekhin version. We interpret this as indicating that the Haensel-Prószyński version is more reliable, at least for our situation. (There is also a more involved thermodynamically consistent interpolation method due to Swesty [85], but we have not experimented with this.)
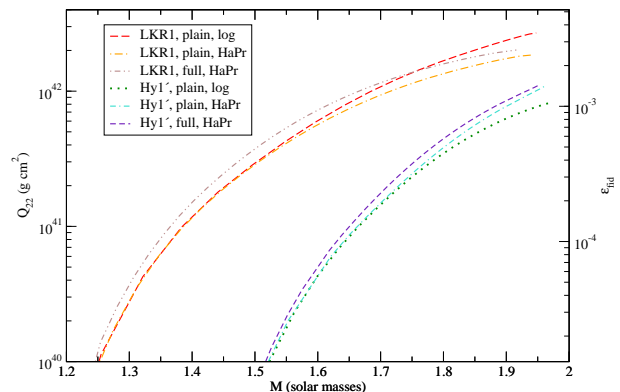

FIG. 11: The full relativistic maximum quadrupole deformations (and fiducial ellipticity) of hybrid stars versus mass, for the LKR1 and Hy1′ EOSs from [29], with a surface tension of $\sigma = 80$ MeV fm^{-2}, showing the effects of the different interpolation methods and EOS additions. Here, "plain" denotes no additions, while "full" denotes both blob and lattice additions. Similarly, "log" and "HaPr" denote the standard logarithmic and Haensel-Prószyński interpolation, respectively. Note that many of the curves end somewhat short of the maximum mass, due to difficulties with the numerics.

We show the differences in the final stellar quantities calculated using the logarithmic and Haensel-Prószyński interpolation for the case of no EOS additions, as well as the effects of the EOS additions with the Haensel-Prószyński interpolation in Table I. (The $\lesssim 0.5\%$ differences in the maximum mass due to the different methods of interpolation are in line with the differences found by Haensel and Prószyński [84], though they find an increase in the maximum mass, while we only find decreases.) Additionally, including the EOS additions and changing the interpolation also has an effect on the maximum

	σ (MeV fm^{-2})	interpolation	EOS additions	$M_{\max}$ ($M_\odot$)	$M_{\min}^{\text{hybrid}}$ ($M_\odot$)	$R_{\max}^{\text{hybrid}}/R$ (%)	$\mathcal{C}_{\max}$	densest hybrid phase
	–	log	none	2.057	1.747	57.7	0.484	Q, $d = 1.03$
Hy1	–	HaPr	none	2.047	1.743	57.6	0.484	Q, $d = 1.05$
	80	HaPr	blob + lattice	2.040	1.742	57.4	0.483	Q, $d = 1.03$
	–	log	none	1.974	1.377	69.0	0.476	H, $d = 1.30$
Hy1$'$	–	HaPr	none	1.963	1.375	69.0	0.476	H, $d = 1.24$
	80	HaPr	blob + lattice	1.955	1.375	68.9	0.475	H, $d = 1.27$
	–	log	none	1.955	1.096	72.5	0.433	H, $d = 3.00$
LKR1	–	HaPr	none	1.948	1.098	72.4	0.433	H, $d = 3.00$
	80	HaPr	blob + lattice	1.935	1.098	72.3	0.431	H, $d = 3.00$
	–	log	none	1.986	1.878	44.0	0.500	Q, $d = 2.10$
generic	–	HaPr	none	1.974	1.869	43.8	0.500	Q, $d = 2.12$
	80	HaPr	blob + lattice	1.971	1.869	43.4	0.499	Q, $d = 2.15$
	–	log	none	1.974	1.534	65.9	0.515	Q, $d = 1.36$
generic$'$	–	HaPr	none	1.963	1.528	65.9	0.515	Q, $d = 1.36$
	80	HaPr	blob + lattice	1.959	1.528	65.8	0.514	Q, $d = 1.38$

TABLE I: Properties of stable stars constructed with the EOSs from [29] (except for the different Hy1 "flavors"), showing the effects of the interpolation and the additions to the EOS. In the "interpolation" column, "log" denotes the standard logarithmic interpolation of the EOS table (used to obtain the values for stellar quantities given in Table I of [29], which we repeat here, with the small corrections from the erratum), while "HaPr" denotes the Haensel-Prószyński thermodynamically consistent interpolation. In the "EOS additions" column, "blob + lattice" denotes the case where we have included the blob and lattice energy densities and lattice pressure in the EOS. The other columns are the same as in Table I of [29]. Explicitly, $M_{\min}^{\text{hybrid}}$ gives the masses of stars that first contain hybrid matter (using the binding energy argument); $R_{\max}^{\text{hybrid}}/R$ denotes the maximum radius fraction occupied by hybrid matter (i.e., the radius fraction for the maximum mass star); and $\mathcal{C}_{\max}$ denotes the maximum compactness ($2GM/Rc^2$) of a star. We also give the composition of the rare phase ("Q" stands for quark and "H" for hadronic) and the dimension of the lattice at the center of the maximum mass star. (Note that is often necessary to locate the maximum mass with more than its given accuracy to obtain $R_{\max}^{\text{hybrid}}/R$, $\mathcal{C}_{\max}$, and the dimension of the densest hybrid phase to their given accuracy, as discussed in the erratum to [29].)

quadrupoles (at most $\sim 40\%$), illustrated in Fig. 11 for the two EOSs that yield the largest quadrupoles.

The EOS additions and Haensel-Prószyński interpolation both reduce the maximum mass, compared to the plain logarithmic interpolation results. Thus, EOSs that already have a low maximum mass (particularly LKR1) with the logarithmic interpolation and no additions may no longer be consistent within 1σ with observations of massive neutron stars when using the Haensel-Prószyński interpolation and including the additions. Indeed, these EOSs were designed to be compatible with the Demorest *et al.* observation of a $1.97\pm0.04\,M_\odot$ neutron star [86], so some of them (again, particularly LKR1) are not compatible within 1σ with the very recent observation of a $2.01 \pm 0.04\,M_\odot$ neutron star by Antoniadis *et al.* [87], even with no additions and the logarithmic interpolation. Nevertheless, all of them are still compatible within 2σ, even with the additions and Haensel-Prószyński interpolation. It is also worth pointing out that the Antoniadis *et al.* measurement is less clean than the Demorest *et al.* measurement, as it relies on some modeling of white dwarf atmospheres, not just geometrical considerations.

Additionally, one can easily obtain 1σ compatibility with the Antoniadis *et al.* measurement with a slight modification of the EOS parameters. For instance, for the LKR1 EOS, changing the QCD coupling constant α_s from 0.6 to 0.625 increases the maximum mass to $2.004\,M_\odot$ with the logarithmic interpolation and no additions and to $1.984\,M_\odot$ with the Haensel-Prószyński interpolation and additions (with a surface tension of $\sigma = 80$ MeV fm^{-2}), while only decreasing the maximum quadrupoles by $\lesssim 30\%$ for the largest masses

Finally, we describe exactly how we obtain the lattice contributions to the EOS. We compute the lattice and cell energy density [$(E_{\text{cell}}+W)/\Omega$] using Eqs. (2) and (14) in [29] and the electrostatic pressure contribution by multiplying that paper's Eq. (20) by $d/3$ to account for the angle-averaged anisotropy (d is the dimension of the lattice). We have also experimented with adding in the isotropic contribution to the pressure from changing the cell energy and blob's charge, given by $-(E_{\text{cell}} + 2W)/\Omega$. We found that this addition does not change the qualitative conclusions, and, indeed, makes the mixed phase even more strongly favored, giving some indication of the robustness of the calculation.

[1] I. S. Shklovskii, Astron. Zh. **46**, 715 (1969).

[2] J. P. Ostriker and J. E. Gunn, Astrophys. J. **157**, 1395

(1969).

[3] A. Ferrari and R. Ruffini, Astrophys. J. Lett. **158**, L71 (1969).

[4] H. J. Melosh, Nature (London) **224**, 781 (1969).

[5] W. H. Press and K. S. Thorne, Annu. Rev. Astron. Astrophys. **10**, 335 (1972).

[6] B. P. Abbott *et al.* (LIGO Scientific Collaboration and Virgo Collaboration), Astrophys. J. **713**, 671 (2010).

[7] J. Abadie *et al.* (LIGO Scientific Collaboration), Astrophys. J. **722**, 1504 (2010).

[8] J. Abadie *et al.* (LIGO Scientific Collaboration and Virgo Collaboration), Astrophys. J. **737**, 93 (2011).

[9] B. J. Owen, Classical Quantum Gravity **26**, 204014 (2009).

[10] M. Pitkin, Mon. Not. R. Astron. Soc. **415**, 1849 (2011).

[11] P. Astone (for the LIGO Scientific Collaboration and Virgo Collaboration), Classical Quantum Gravity **29**, 124011 (2012).

[12] B. J. Owen, Phys. Rev. Lett. **95**, 211101 (2005).

[13] K. Ioka and M. Sasaki, Astrophys. J. **600**, 296 (2004).

[14] R. Ciolfi, V. Ferrari, and L. Gualtieri, Mon. Not. R. Astron. Soc. **406**, 2540 (2010).

[15] S. Yoshida, K. Kiuchi, and M. Shibata, Phys. Rev. D **86**, 044012 (2012).

[16] J. Frieben and L. Rezzolla, Mon. Not. R. Astron. Soc. **427**, 3406 (2012).

[17] R. Ciolfi and L. Rezzolla, arXiv:1306.2803 [astro-ph.SR].

[18] G. Ushomirsky, C. Cutler, and L. Bildsten, Mon. Not. R. Astron. Soc. **319**, 902 (2000).

[19] L.-M. Lin, Phys. Rev. D **76**, 081502(R) (2007).

[20] B. Knippel and A. Sedrakian, Phys. Rev. D **79**, 083007 (2009).

[21] C. J. Horowitz, Phys. Rev. D **81**, 103001 (2010).

[22] B. Haskell, D. I. Jones, and N. Andersson, Mon. Not. R. Astron. Soc. **373**, 1423 (2006).

[23] B. Haskell, N. Andersson, D. I. Jones, and L. Samuelsson, Phys. Rev. Lett. **99**, 231101 (2007).

[24] F. Douchin and P. Haensel, Astron. Astrophys. **380**, 151 (2001).

[25] S. Ogata and S. Ichimaru, Phys. Rev. A **42**, 4867 (1990).

[26] C. J. Horowitz and J. Hughto, arXiv:0812.2650 [astro-ph].

[27] D. A. Baiko, Mon. Not. R. Astron. Soc. **416**, 22 (2011).

[28] D. A. Baiko, Contrib. Plasma Phys. **52**, 157 (2012).

[29] N. K. Johnson-McDaniel and B. J. Owen, Phys. Rev. D **86**, 063006 (2012), **87**, 129903(E) (2013).

[30] M. Mannarelli, K. Rajagopal, and R. Sharma, Phys. Rev. D **76**, 074026 (2007).

[31] A. Kurkela, P. Romatschke, and A. Vuorinen, Phys. Rev. D **81**, 105021 (2010).

[32] C. J. Horowitz and K. Kadau, Phys. Rev. Lett. **102**, 191102 (2009).

[33] K. Hoffman and J. Heyl, Mon. Not. R. Astron. Soc. **426**, 2404 (2012).

[34] A. I. Chugunov and C. J. Horowitz, Mon. Not. R. Astron. Soc. Lett. **407**, L54 (2010).

[35] B. Carter and H. Quintana, Proc. R. Soc. A **331**, 57 (1972).

[36] M. Karlovini and L. Samuelsson, Classical Quantum Gravity **20**, 3613 (2003), **22**, 771(E) (2005).

[37] B. L. Schumaker and K. S. Thorne, Mon. Not. R. Astron. Soc. **203**, 457 (1983).

[38] K. S. Thorne and A. Campolattaro, Astrophys. J. **149**, 591 (1967), **152**, 673(E) (1968).

[39] T. Regge and J. A. Wheeler, Phys. Rev. **108**, 1063 (1957).

[40] T. Hinderer, Astrophys. J. **677**, 1216 (2008), **697**, 964(E) (2009).

[41] É. É. Flanagan and T. Hinderer, Phys. Rev. D **77**, 021502(R) (2008).

[42] J. R. Ipser, Astrophys. J. **166**, 175 (1971).

[43] K. S. Thorne, Rev. Mod. Phys. **52**, 299 (1980).

[44] P. Musgrave, D. Pollney, and K. Lake, computer code GRTensorII (1996), `http://grtensor.phy.queensu.ca/`.

[45] L. Lindblom, G. Mendell, and B. J. Owen, Phys. Rev. D **60**, 064006 (1999).

[46] G. B. Arfken and H. J. Weber, *Mathematical Methods for Physicists* (Elsevier, Boston, 2005), 6th ed.

[47] R. M. Wald, *General Relativity* (University of Chicago Press, Chicago, 1984).

[48] P. Haensel and A. Y. Potekhin, Astron. Astrophys. **428**, 191 (2004).

[49] P. Haensel, A. Y. Potekhin, and D. G. Yakovlev, *Neutron Stars 1: Equation of State and Structure* (Springer, New York, 2007).

[50] `http://www.ioffe.ru/astro/NSG/NSEOS/`.

[51] G. Baym, C. Pethick, and P. Sutherland, Astrophys. J. **170**, 299 (1971).

[52] J. W. Negele and D. Vautherin, Nucl. Phys. A **207**, 298 (1973).

[53] J. M. Lattimer and M. Prakash, Astrophys. J. **550**, 426 (2001).

[54] A. Kurkela, P. Romatschke, A. Vuorinen, and B. Wu, arXiv:1006.4062 [astro-ph.HE].

[55] `http://theory.physics.helsinki.fi/~aekurkel/neutron/`.

[56] L. Lindblom, Astrophys. J. **398**, 569 (1992).

[57] P. Haensel, in *Physics of Neutron Star Interiors*, edited by D. Blaschke, A. Sedrakian, and N. K. Glendenning (Springer, Berlin, 2001), vol. 578 of *Lecture Notes in Physics*, p. 127.

[58] J. M. Lattimer, Annu. Rev. Nucl. Part. Sci. **62**, 485 (2012), URL `http://stellarcollapse.org/nsmasses`.

[59] N. K. Johnson-McDaniel, arXiv:1303.3259 [astro-ph.SR].

[60] A. J. Penner, N. Andersson, L. Samuelsson, I. Hawke, and D. I. Jones, Phys. Rev. D **84**, 103006 (2011).

[61] R. Hill, Proc. Phys. Soc. London Sect. A **65**, 349 (1952).

[62] C. J. Pethick and A. Y. Potekhin, Phys. Lett. B **427**, 7 (1998).

[63] S. B. Rüster, M. Hempel, and J. Schaffner-Bielich, Phys. Rev. C **73**, 035804 (2006).

[64] `http://phys-merger.physik.unibas.ch/~hempel/eos.html`.

[65] M. B. Pinto, V. Koch, and J. Randrup, Phys. Rev. C **86**, 025203 (2012).

[66] T. Hinderer, B. D. Lackey, R. N. Lang, and J. S. Read, Phys. Rev. D **81**, 123016 (2010).

[67] T. Damour and A. Nagar, Phys. Rev. D **80**, 084035 (2009).

[68] `http://hep.itp.tuwien.ac.at/~paulrom/eost0/eospaper.html`.

[69] M. G. Alford, A. Schmitt, K. Rajagopal, and T. Schäfer, Rev. Mod. Phys. **80**, 1455 (2008).

[70] K. Rajagopal and E. Shuster, Phys. Rev. D **62**, 085007 (2000).

[71] T. Binnington and E. Poisson, Phys. Rev. D **80**, 084018

(2009).

[72] S. Postnikov, M. Prakash, and J. M. Lattimer, Phys. Rev. D **82**, 024016 (2010).

[73] W. G. Newton, M. Gearheart, and B.-A. Li, Astrophys. J. Suppl. Ser. **204**, 9 (2013).

[74] M. Gearheart, W. G. Newton, J. Hooker, and B.-A. Li, Mon. Not. R. Astron. Soc. **418**, 2343 (2011).

[75] A. Corsi and B. J. Owen, Phys. Rev. D **83**, 104014 (2011).

[76] B. F. Schutz, Jr., Astrophys. J. Suppl. Ser. **24**, 343 (1972).

[77] S. L. Detweiler and J. R. Ipser, Astrophys. J. **185**, 685 (1973).

[78] L. S. Finn, Mon. Not. R. Astron. Soc. **245**, 82 (1990).

[79] J. P. Watt, G. F. Davies, and R. J. O'Connell, Rev. Geophys. Space Phys. **14**, 541 (1976).

[80] H. Heiselberg, C. J. Pethick, and E. F. Staubo, Phys.

[81] Rev. Lett. **70**, 1355 (1993).

[81] M. Alford, K. Rajagopal, S. Reddy, and F. Wilczek, Phys. Rev. D **64**, 074017 (2001).

[82] M. B. Christiansen and N. K. Glendenning, Phys. Rev. C **56**, 2858 (1997).

[83] M. B. Christiansen and N. K. Glendenning, astro-ph/0008207.

[84] P. Haensel and M. Prószyński, Astrophys. J. **258**, 306 (1982).

[85] F. D. Swesty, J. Comput. Phys. **127**, 118 (1996).

[86] P. B. Demorest, T. Pennucci, S. M. Ransom, M. S. E. Roberts, and J. W. T. Hessels, Nature (London) **467**, 1081 (2010).

[87] J. Antoniadis *et al.*, Science **340**, 1233232 (2013).